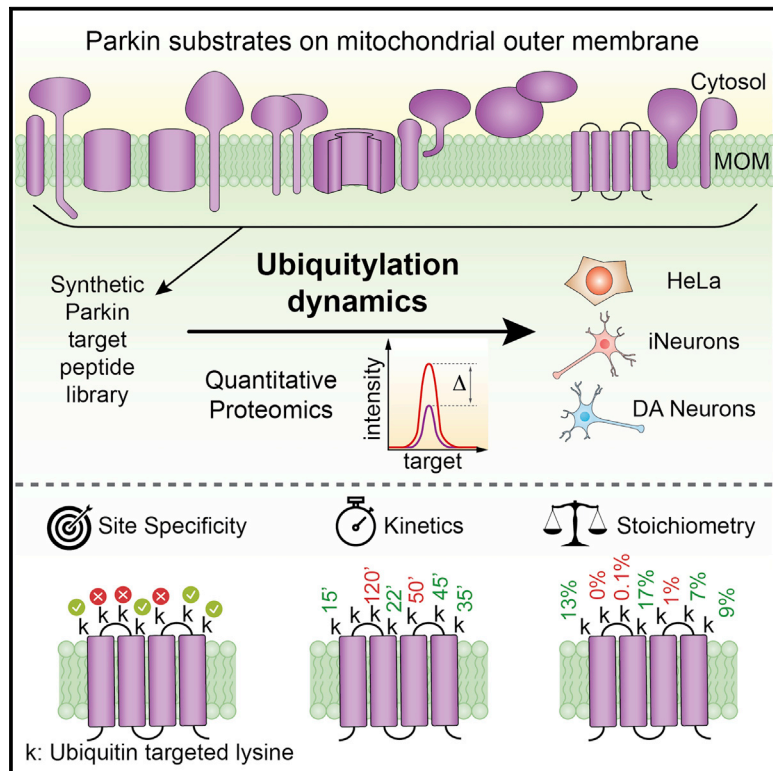


Dynamics of PARKIN-Dependent Mitochondrial Ubiquitylation in Induced Neurons and Model Systems Revealed by Digital Snapshot Proteomics

Graphical Abstract



Authors

Alban Ordureau, Joao A. Paulo, Wei Zhang, ..., Sachdev S. Sidhu, Steven P. Gygi, J. Wade Harper

Correspondence

wade_harper@hms.harvard.edu

In Brief

The PARKIN ubiquitin ligase is activated on damaged mitochondria via the PINK1 kinase, where it ubiquitylates an array of proteins. Ordureau et al. develop a quantitative proteomics approach to measure the dynamics, site specificity, and stoichiometry of PARKIN-dependent substrate ubiquitylation in neuronal cells, providing a quantitative analysis of the pathway.

Highlights

- Quantification of PARKIN-dependent Ub signaling on mitochondria in neurons
- PARKIN displays dramatic Lys site specificity within targets
- PARKIN^{S65} phosphorylation by PINK1 is required for feedforward activation in neurons
- Stoichiometry of Ub phosphorylation *in vivo* optimized for mitophagy receptor binding



Dynamics of PARKIN-Dependent Mitochondrial Ubiquitylation in Induced Neurons and Model Systems Revealed by Digital Snapshot Proteomics

Alban Ordureau,¹ Joao A. Paulo,¹ Wei Zhang,² Tim Ahfeldt,^{3,4} Jiuchun Zhang,¹ Erin F. Cohn,^{1,5} Zhonggang Hou,^{1,6} Jin-Mi Heo,¹ Lee L. Rubin,³ Sachdev S. Sidhu,² Steven P. Gygi,¹ and J. Wade Harper^{1,7,*}

¹Department of Cell Biology, Harvard Medical School, Boston, MA 02115, USA

²Donnelly Centre for Cellular and Biomolecular Research, Banting and Best Department of Medical Research, and Department of Molecular Genetics, University of Toronto, 160 College Street, Toronto, ON M5S3E1, Canada

³Department of Stem Cell and Regenerative Biology, Harvard University, Cambridge, MA 02132, USA

⁴Present address: Department of Neuroscience, Icahn School of Medicine at Mount Sinai, New York, NY 10029, USA

⁵Present address: School of Medicine, Case Western Reserve University, Cleveland, OH 44106, USA

⁶Present address: Department of Biological Chemistry, University of Michigan, Ann Arbor, MI 48109, USA

⁷Lead Contact

*Correspondence: wade_harper@hms.harvard.edu

<https://doi.org/10.1016/j.molcel.2018.03.012>

SUMMARY

Flux through kinase and ubiquitin-driven signaling systems depends on the modification kinetics, stoichiometry, primary site specificity, and target abundance within the pathway, yet we rarely understand these parameters and their spatial organization within cells. Here we develop temporal digital snapshots of ubiquitin signaling on the mitochondrial outer membrane in embryonic stem cell-derived neurons, and we model HeLa cell systems upon activation of the PINK1 kinase and PARKIN ubiquitin ligase by proteomic counting of ubiquitylation and phosphorylation events. We define the kinetics and site specificity of PARKIN-dependent target ubiquitylation, and we demonstrate the power of this approach to quantify pathway modulators and to mechanistically define the role of PARKIN UBL phosphorylation in pathway activation in induced neurons. Finally, through modulation of pS65-Ub on mitochondria, we demonstrate that Ub hyper-phosphorylation is inhibitory to mitophagy receptor recruitment, indicating that pS65-Ub stoichiometry *in vivo* is optimized to coordinate PARKIN recruitment via pS65-Ub and mitophagy receptors via unphosphorylated chains.

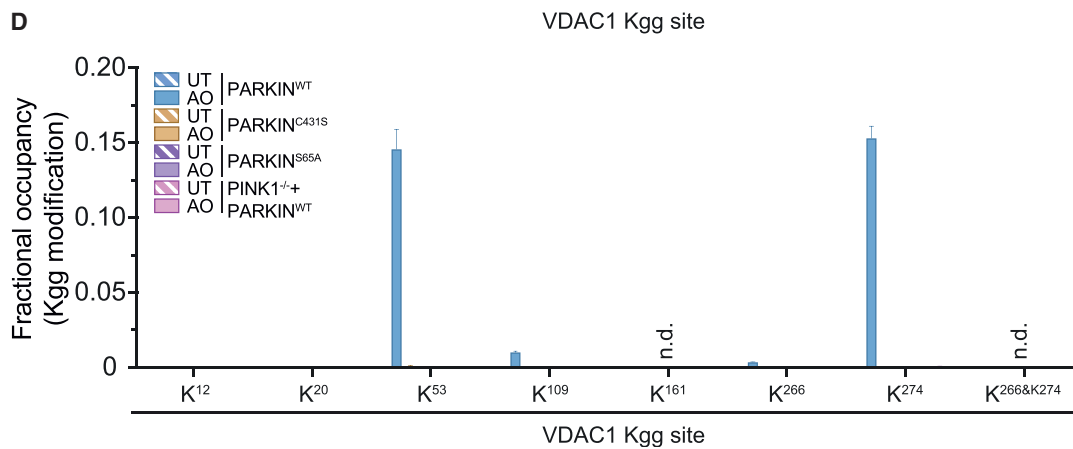
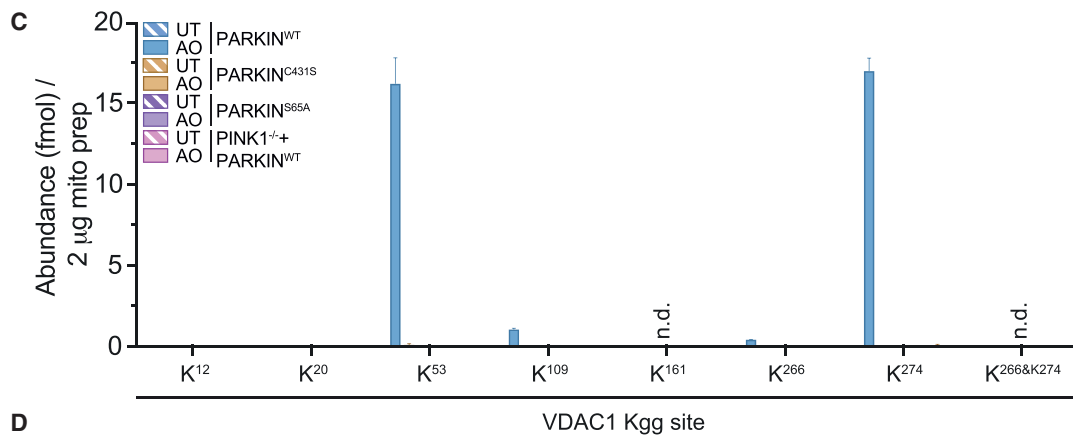
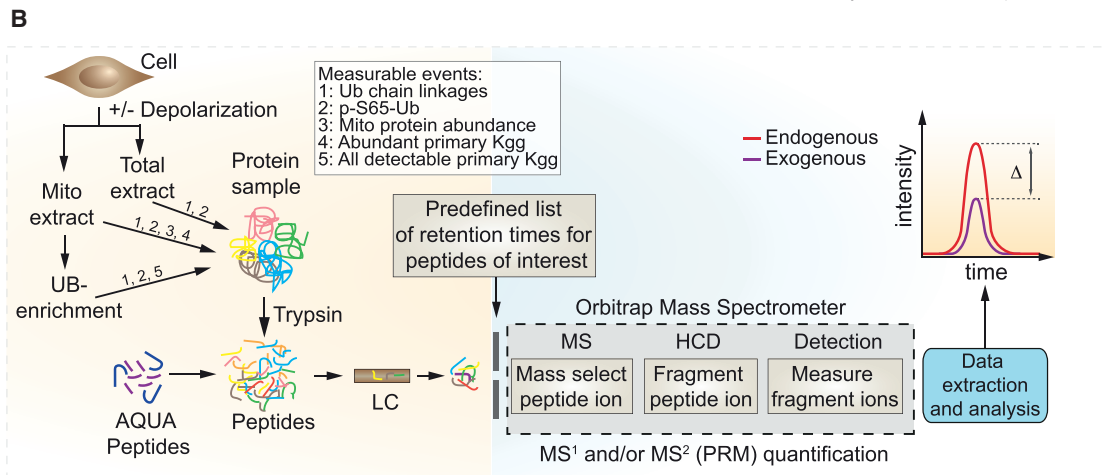
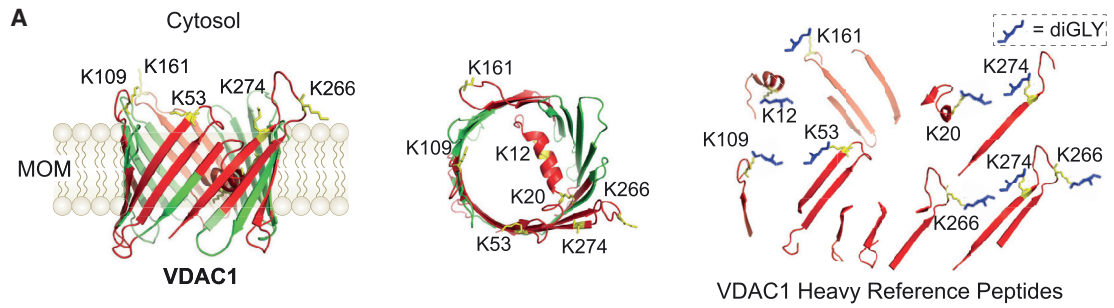
INTRODUCTION

Cellular decisions often involve the coordination of protein kinase- and ubiquitin (Ub) ligase-driven signaling networks (Hunter, 2007). While network architecture varies, three features generally apply: (1) signals are propagated in space and time within the cell, often with feedback control; (2) both kinases

and Ub ligases often modify multiple target sites on diverse proteins within a pathway in a distributive manner, sometimes involving multiple Ub chain linkage types (Kulathu and Komander, 2012); and (3) pathway flux depends on modification stoichiometry within individual pools of target proteins. However, we rarely understand the extent to which complex modifications within a pathway are spatially or kinetically distinguishable, due in part to the absence of antibodies that can reveal site specificity and kinetics. Here we develop targeted Kgg remnant and phospho-proteomics as a means by which to provide digital snapshots of primary site specificity, kinetics, and stoichiometry of the individual modification events in a dynamic kinase- and Ub ligase-driven signaling cascade critical for mitochondrial quality control.

Mitochondrial oxidative or proteotoxic stress can promote the removal of damaged mitochondria through a form of selective autophagy called mitophagy, requiring the PARKIN RING-Between-RING (RBR) Ub ligase and mitochondrially localized protein kinase PINK1, both found mutated in Parkinson's disease (reviewed in Pickrell and Youle, 2015; Yamano et al., 2016). When mitochondria are healthy, PINK1 abundance in mitochondria is low and PARKIN is localized in the cytosol in an auto-inhibited form (Pickrell and Youle, 2015). In response to mitochondrial damage, PINK1 accumulates on the mitochondrial outer membrane (MOM) (Lazarou et al., 2012; Narendra et al., 2010b; Yamano and Youle, 2013) where it promotes PARKIN recruitment to mitochondria and activation of MOM protein ubiquitylation through a complex feedforward mechanism involving the following: (1) phosphorylation of S65 in Ub chains on the MOM with a stoichiometry of ~0.2 in the HeLa cell system, (2) phosphorylation of S65 in PARKIN's Ub-like (UBL) domain to greatly enhance its ligase activity by reversal of auto-inhibition, and (3) binding of PARKIN to pS65-Ub chains to both retain it on the MOM and promote UBL phosphorylation by PINK1 (Kane et al., 2014; Kazlauskaitė et al., 2014a, 2014b, 2015; Koyano et al., 2014; Narendra et al., 2008; Okatsu et al., 2015; Ordureau et al., 2014, 2015; Wauer et al., 2015a). Retention of





(legend on next page)

active PARKIN on the MOM results in ubiquitylation of numerous substrates (Bingol et al., 2014; Rose et al., 2016; Sarraf et al., 2013) and the assembly of Ub chains that serve to recruit autophagy receptors and promote downstream steps in mitophagy (Pickrell and Youle, 2015; Yamano et al., 2016).

Despite these advances, numerous gaps exist in our understanding of the dynamics and sequence of steps in the process of MOM ubiquitylation by PARKIN (reviewed in Harper et al., 2018). First, we do not understand the extent to which PARKIN acts in a site-specific manner to ubiquitylate Lys residues in target proteins, nor do we know what role substrate abundance plays in MOM ubiquitylation. Previous studies identifying PARKIN primary ubiquitylation sites employed cell lines with varied PARKIN levels and a wide range of depolarization times. This, coupled with the stochastic nature of antibody-directed Kgg peptide identification, greatly limits our understanding of the relative rates of ubiquitylation of individual primary sites in PARKIN targets. Second, to date, the kinetics and specificity of PARKIN target ubiquitylation has not been examined in neuronal cells, and we therefore do not know the extent to which target ubiquitylation parallels that seen in the PARKIN-overexpressing HeLa cell system. Third, the relative contributions of Ub and PARKIN phosphorylation by PINK1 in promoting the feedforward process *in vivo* are poorly understood. The available data in HeLa cell systems present a paradox: on one hand, PARKIN mutants that are unable to bind pS65-Ub are unable to promote MOM ubiquitylation, suggesting that this interaction is important for retention of PARKIN on damaged mitochondria (Kazlauskaite et al., 2015; Wauer et al., 2015a). In addition, binding of PARKIN to pS65-Ub can dramatically promote PINK1-dependent phosphorylation of PARKIN's UBL *in vitro*, suggesting that recruitment of unphosphorylated PARKIN to pre-existing pS65-Ub on the MOM can promote both PARKIN recruitment and activation (Kazlauskaite et al., 2015; Wauer et al., 2015a). On the other hand, catalytically inactive PARKIN that is defective in the assembly of Ub chains on the MOM is also not retained, suggesting that new Ub chain synthesis by PARKIN is required for the feedforward process (Fiesel et al., 2015; Lazarou et al., 2013; Narendra et al., 2008; Ordureau et al., 2014). Finally, the form of Ub chains that are used to recruit Ub-binding autophagy receptors such as OPTN to the MOM is unclear, with evidence for and against direct involvement of pS65-Ub in receptor recruitment (Lazarou et al., 2015; Ordureau et al., 2015; Richter et al., 2016; reviewed in Harper et al., 2018).

Here we report the development of a PARKIN target-Parallel Reaction Monitoring (Pt-PRM) platform that allows quantitative proteomic snapshots of site-specific primary ubiquitylation for

15 MOM proteins, target protein abundance, Ub chain assembly, and Ub phosphorylation during early steps in PARKIN-dependent mitophagy. First, we employ Pt-PRM to generate temporal snapshots of PARKIN activity in the widely used HeLa cell system, thereby defining kinetic preferences for site-specific ubiquitylation and the relationship between ubiquitylation rates and target abundance. Second, we demonstrate that Pt-PRM can be used to quantify the effects of a small-molecule PINK1 activator and newly evolved inhibitory Ub variant (UbV) proteins targeting PARKIN. Third, we employ human embryonic stem cell (hESC)-derived NGN2-induced neurons (iNeurons) and dopaminergic (DA) neurons to provide the first quantitative analysis of endogenous PARKIN target ubiquitylation in induced neurons, revealing similarities and differences with the HeLa system. Fourth, using hESCs gene edited to express PARKIN^{S65A}, we quantitatively assess the questioned role of PARKIN UBL phosphorylation in target ubiquitylation, Ub S65 phosphorylation, and PARKIN recruitment to the MOM in iNeurons, thereby demonstrating a critical role for this modification in the initiation of the feedforward process. Finally, we use this platform to evaluate the role of pS65-Ub in downstream recruitment of Ub-binding mitophagy receptors (Lazarou et al., 2015; Ordureau et al., 2015; Richter et al., 2016; reviewed in Harper et al., 2018), finding that an increase in pS65-Ub stoichiometry from ~0.2 to 0.5–0.65 *in vivo* is inhibitory to mitophagy receptor recruitment, thereby suggesting that the fractional occupancy of Ub chain phosphorylation *in vivo* with endogenous PINK1 levels is optimized for PARKIN and mitophagy receptor recruitment. This work reveals the power of pathway-directed PRM for capturing digital snapshots of Ub and phosphorylation-driven signaling systems, and it sets the stage for understanding the molecular mechanisms of Parkinson's disease and other neurodegenerative disease-signaling pathways using quantitative analysis of induced neurons.

RESULTS

Quantitative Analysis of Site-Specific VDAC1 Ubiquitylation by PARKIN

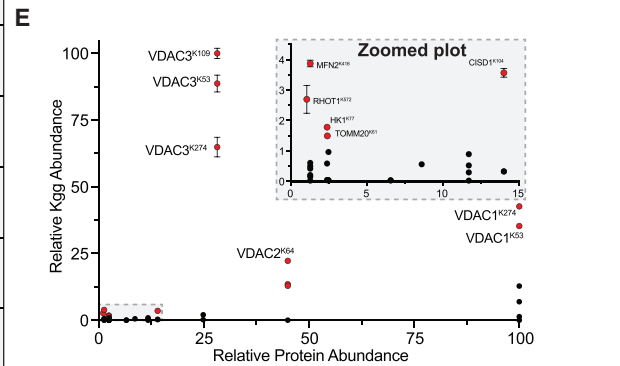
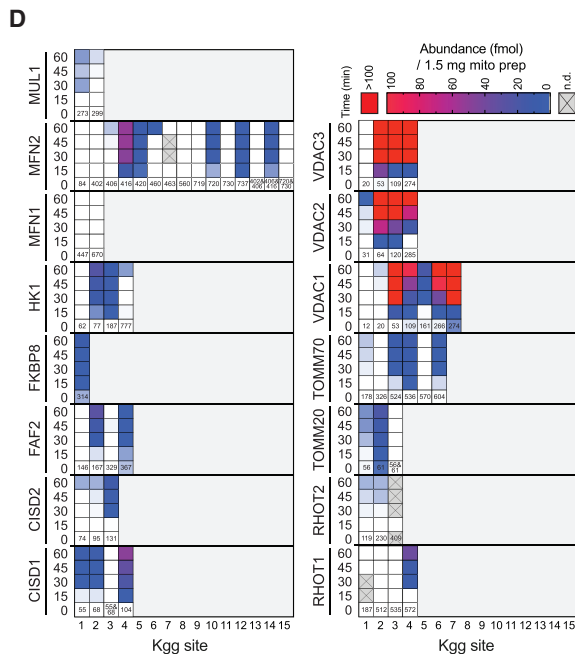
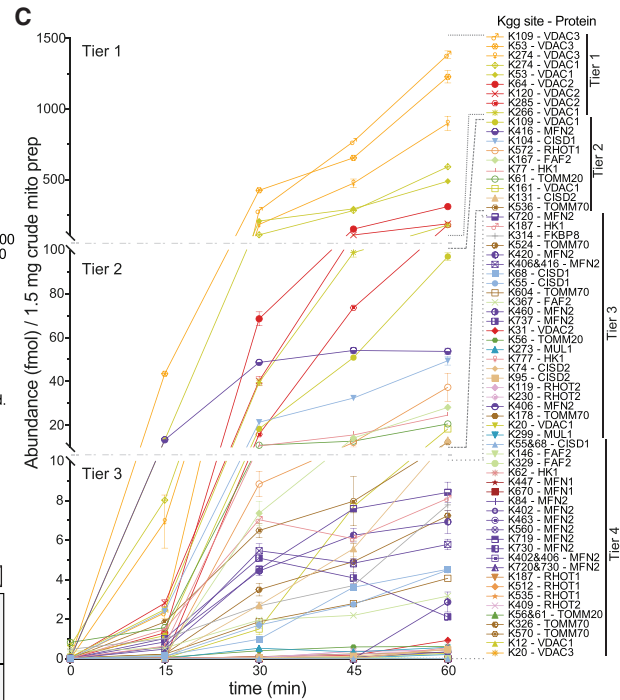
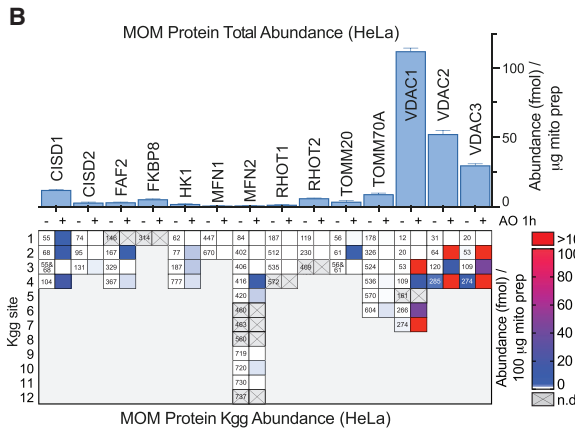
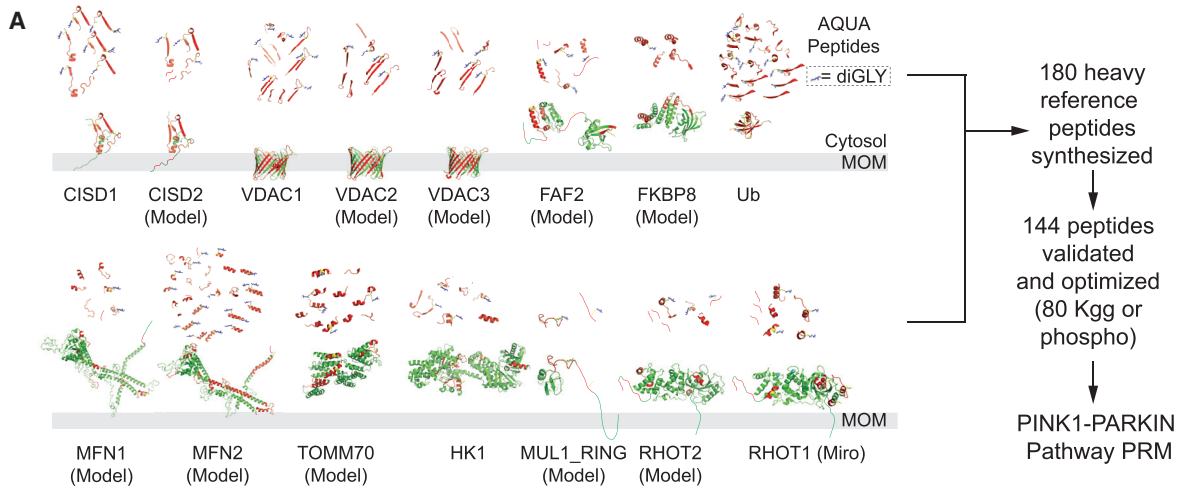
VDACs are β -barrel proteins embedded within the MOM. Four cytosolic loops in VDAC1, as well as an N-terminal α helix, contain a total of 7 Lys residues, some of which have been detected as candidate PARKIN ubiquitylation sites using Kgg capture proteomics (Bingol et al., 2014; Rose et al., 2016; Sarraf et al., 2013); and, as we show below, VDAC1 is one of the most strongly ubiquitylated PARKIN substrates. We optimized a series of heavy reference peptides for PRM of all 7 potential individual ubiquitylation sites (Kgg remnant-containing peptides), a potential doubly modified peptide, and unmodified

Figure 1. Quantitative Analysis of VDAC1 Ubiquitylation on Mitochondria in Response to PARKIN Activation

(A) Location of 7 candidate PARKIN-targeted Lys residues (yellow) in VDAC1. The right panel shows VDAC1 tryptic heavy reference peptides (red) containing Kgg sites, blue), as well as 3 Lys-free peptides for measurement of VDAC1 abundance.

(B) Scheme for PRM analysis. Cell extracts, enriched mitochondria, or ubiquitylated proteins from mitochondria purified on immobilized UBA resins are trypsinized and mixed with heavy reference peptides corresponding to phospho or Kgg-containing tryptic peptides or unmodified peptides prior to analysis by proteomics. MS¹ and MS² intensities are used to determine relative and absolute abundance of individual sites or protein using Skyline (MacLean et al., 2010). (C and D) Cell lines were depolarized for 1 hr with AO, and mitochondria were isolated and subjected to PRM analysis. The abundance (fmol) of Kgg peptides (C) and the fractional occupancy (D) for individual sites are shown. Error bars represent SEM (n = 3). n.d., not determined.

See also Figure S1 and Table S2.



(legend on next page)

peptides for measurement of VDAC1 abundance (Figures 1A and S1A–S1C; Table S1). The general scheme for the PRM platform is shown in Figure 1B. HeLa Flip-In T-REx cells engineered to inducibly express a single copy of PARKIN^{WT}, the catalytically defective PARKIN^{C431S} mutant, or a non-phosphorylatable PARKIN^{S65A} mutant under a doxycyclin-inducible promoter (with or without PINK1) were depolarized with antimycin A/oligomycin A (AO) for 1 hr. Isolated mitochondria were either: (1) employed for direct proteomic analysis of VDAC1 protein, Ub phosphorylation, and ubiquitylation of abundant primary Kgg sites; or (2) enriched for all ubiquitylated proteins using sequential binding to Halo-immobilized tandem UBA domains from UBQLN1 (4X) and DSK2 (5X) to facilitate recovery of low-abundance Kgg species (see STAR Methods) prior to PRM proteomics (Figures 1B, S1A, and S1B). Association of these resins with mono-Ub, K48 chains, and K63 chains was not affected by stoichiometric phosphorylation on S65 (Figure S1D).

The most abundant PARKIN and depolarization-dependent VDAC1 Kgg peptides contained K53 and K274, and the extent of ubiquitylation of K109 and K266 was ~20-fold lower (Figure 1C). Under these conditions, ubiquitylation of K12 or K20, as well as ubiquitylation to yield the doubly modified K266/K274 peptide, was below the detection limit. Ubiquitylation of these sites was dependent upon PINK1, the catalytic C341 in PARKIN, and the PINK1 phosphorylation site in PARKIN's UBL (Figure 1C). We determined a fractional occupancy of ~0.15 for modification of K53 and K274 and <0.01 for K109 and K266 (Figure 1D). Given that these modifications are unlinked after trypsinization, it isn't clear if individual VDAC1 molecules are primarily singly or doubly modified, and the extent to which the multiply ubiquitylated forms observed by immunoblotting of UBA resin-enriched VDAC1 reflect multi-mono-ubiquitylation, Ub chain extension, or both is unclear (Figures 1C and S1E). Thus, PARKIN has a preference for ubiquitylating a subset of Lys residues in cytosolic loops of VDAC1's β -barrel, while Lys residues located within the α -helical N terminus (Figure 1A) are not detectably targeted under these conditions.

Development of a Pt-PRM Platform

Given the ability to examine the dynamics of VDAC1 ubiquitylation, we developed a robust PRM platform to simultaneously monitor ubiquitylation of a structurally diverse set of candidate PARKIN targets (Bingol et al., 2014; Chan et al., 2011; Rose et al., 2016; Sarraf et al., 2013). We chose 15 candidate substrates, which based on label-free quantification of MOM

proteins, span a 300-fold range in abundance within purified mitochondria, with VDACs being by far the most abundant and RHOT1 being the least abundant (Figures S1F–S1H; Table S2). From these candidates and Ub itself, we designed 180 heavy reference tryptic peptides corresponding to Kgg-containing peptides, non-ubiquitylated peptides for quantification of total protein abundance, and phospho-peptides for detection of pS65-Ub (Figure 2A; Table S1) (Ordureau et al., 2014; Phu et al., 2011). A total of 144 peptides, including 80 that measure modified states, were validated for their reproducibility and robustness and optimized for PRM measurements (Figures S1A–S1C and S2A; Table S1; see STAR Methods). These parameters were employed in the functional experiments described below.

Digital Snapshot of PARKIN Target Primary Ubiquitylation in HeLa Cells

As a first validation, we compared the abundance of the 15 MOM proteins represented by the Pt-PRM peptide library to the results of label-free abundance for mitochondria from HeLa cells, finding similar relative levels ($R^2 = 0.98$) (Figures 2B and S2B). We enriched ubiquitylated proteins from crude mitochondria (100 μ g) derived from cells with or without depolarization (1 hr) using immobilized UBA domains (Figure 1B), and we performed Pt-PRM (Figure 2B). We detected 25 primary ubiquitylation sites in 9 PARKIN targets that were increased upon depolarization, with detection limits in the ~0.1–1 fmol range (Figure 2B). By far, preferred sites on the three VDAC proteins (equivalent to K53 and K274 in VDAC1) received the largest quantity of primary ubiquitylation across all the substrates tested. A subset of sites on moderate-to-low-abundance substrates MFN2, CISD1, and TOMM20 was also detected (Figure 2B). Thus, Pt-PRM can simultaneously measure site-specific ubiquitylation of diverse PARKIN targets.

To examine the temporal order of site-specific ubiquitylation and increase sensitivity, we performed Pt-PRM on samples derived from purified mitochondria (1.5 mg) over a time course of depolarization (0–60 min) and after enrichment for ubiquitylated proteins (Figures 2C, 2D, S2C, and S2D). This analysis revealed several features of PARKIN-dependent MOM ubiquitylation. First, modification of particular VDAC sites (equivalent to K53 and K274 in VDAC1) was kinetically preferred, being observed as early as 15 min post-depolarization, and modification of these sites continued to increase over the 60-min time course (tier 1 substrates). Detection of ubiquitylation at this early time point suggests the assay is highly sensitive, as the $t_{1/2}$ for

Figure 2. Quantitative Kinetic and Multiplexed Analysis of Site-Specific Mitochondrial Ubiquitylation by PARKIN

(A) Previously determined structures or models of PARKIN targets are shown with individual heavy reference peptide used for Pt-PRM in red (see Table S1 for specific sequences). Non-targeted regions, green; lysines targeted for ubiquitylation, yellow; diGLY residues, blue.

(B) Site-specific ubiquitylation of PARKIN targets on mitochondria upon depolarization. HeLa Flip-In T-REx cells expressing PARKIN^{WT} were left untreated or depolarized with AO (1 hr) prior to Pt-PRM on enriched mitochondria (1 μ g) for total protein abundance or ubiquitylated proteins from enriched mitochondria (100 μ g) for Kgg measurements. Histogram shows protein abundance in 1 μ g mitochondria. Heatmap shows the abundance of target Kgg peptides. Error bars represent SEM (n = 3). n.d., not determined.

(C and D) Kinetics of PARKIN-dependent mitochondrial ubiquitylation. Shown is as in (B), using ubiquitylated proteins from 1.5 mg mitochondria (for each time point post-depolarization) for Pt-PRM; tier clustering (C), and heat map (D). Error bars in (C) represent SEM (n = 3). n.d., not determined.

(E) Correlation plot for the abundance of the most reactive (red) Kgg sites and relative target abundance in mitochondria for the 15 PARKIN targets. Kgg sites indicated in black represent weakly reactive sites. Error bars represent SEM (n = 3).

See also Figure S2 and Table S2.

PARKIN recruitment to mitochondria in this system is 26 min (Ordureau et al., 2014). Second, ubiquitylation of K416 in MFN2 and K61 in TOMM20 was also kinetically preferred (classified as tier 2 substrates), and it was largely maximal by 30 min. Third, a number of substrates accumulated Ub with reduced kinetics, being detectable initially at 30 min post-depolarization (tier 2 and 3 substrates). Fourth, 23 Kgg peptides were not detected even after 60 min of depolarization. Fifth, 8 Kgg peptides were detectable under basal conditions, but, in all cases except one (TOMM70^{K536}), PARKIN promoted further ubiquitylation during the time course (Figure 2C).

To a large degree, ubiquitylation of the most highly preferred sites in individual targets correlated with substrate abundance (red symbols in Figure 2E). Exceptions to this included VDAC3, which displayed a disproportionate level of ubiquitylation on K53, K109, and K274 relative to its abundance, as well as MFN2^{K416} and RHOT1^{K572}. In addition, several substrates of moderate abundance (tenth–15th percentile) had no sites whose ubiquitylation approached expectations based on VDAC1 ubiquitylation rates and abundance (Figure 2E). As with VDAC1, the stoichiometry of the most prominent sites in VDAC2 and 3 ranged from 0.2 to 0.5 (Figure S2E). While the necessity to enrich for low-abundance ubiquitylated PARKIN targets for Kgg detection precludes an accurate determination of stoichiometry, we were able to estimate a fractional occupancy of ~0.1 for the most abundant MFN2 site measured (MFN2^{K416}) (Figures 2C, S2C, and S2D), comparable with the most highly occupied VDAC sites. Other sites on low-abundance PARKIN targets were at or below a stoichiometry of 0.01.

Absence of Extensive Target Turnover in Response to Depolarization

Several studies have reported proteasomal turnover of PARKIN targets in depolarized cells overexpressing PARKIN (Chan et al., 2011; Geisler et al., 2010; Tanaka et al., 2010). However, because target ubiquitylation reduces mobility during SDS-PAGE, this may appear by immunoblotting as a loss of protein abundance. To rigorously examine PARKIN target abundance, we employed the Pt-PRM system with or without depolarization in cells expressing PARKIN^{WT} or PARKIN^{C431S} under the control of a regulated promoter. Across all PARKIN targets examined, we observed no specific loss in protein abundance for any target in response to depolarization (1 hr) in the presence of either PARKIN protein (Figure S2F). Thus, rapid target turnover upon PARKIN-dependent ubiquitylation is not a general feature of the pathway under conditions that generate overt target ubiquitylation (see below).

Pt-PRM for the Assessment of Activators and Inhibitors of the Pathway

We next asked whether Pt-PRM is sufficiently sensitive to quantify PARKIN pathway activators or inhibitors. We initially employed a previously reported PINK1 neo-substrate activator kinetin (Hertz et al., 2013), which enhances the formation of pS65-Ub and mitophagic flux at sub-threshold levels of the mitochondrial depolarizer CCCP (1 μ M) (Figures 3A and S3A). Pathway analysis by Pt-PRM revealed the following: (1) an ~20-fold increase in pS65-Ub formation by kinetin compared with sub-threshold CCCP alone and a maximum Ub phosphorylation stoichiometry of 0.029 on mitochondria (Figure 3B), (2) a 5-fold increase in Ub chain assembly without altering linkage types (Figure 3B), and (3) a dramatic increase in VDAC primary site ubiquitylation (Figure 3C). All of these modifications were absolutely dependent upon PINK1 (Figures 3A–3C). These data indicate that Pt-PRM can be used to quantify the effects of pathway activators and that kinetin enhances PARKIN function without altering its intrinsic preference for chain assembly and target ubiquitylation.

To examine Pt-PRM for monitoring pathway inhibition, we first employed a previously reported UbV phage display library (>10¹⁰ M13 phage) (Zhang et al., 2016) to identify 10 UbVs that bind PARKIN^{295–465} with EC₅₀ values of 0.2–18 nM but do not bind 4 HECT-domain E3s or PARKIN lacking RING2 (Figures S3B–S3G). Each UbV displayed competitive binding with all other UbVs (Figure S3H), and each dramatically inhibited *in vitro* Ub chain assembly pS65-PARKIN (Figure S3I). In the HeLa cell system, 6 of 9 UbVs potently inhibited MFN2 and CISD1 ubiquitylation upon depolarization, largely correlating with EC₅₀ values (Figures 3D and S3G). Analysis of the 3 most potent UbVs using Pt-PRM demonstrated a dramatic reduction in PARKIN-dependent assembly of K6, K11, and K63 Ub chains at 1 and 4 hr post-depolarization, comparable to that seen in cells expressing PARKIN^{C431S} or lacking PINK1 (Figure 3E) (Cunningham et al., 2015; Ordureau et al., 2014, 2015), and concomitant inhibition of VDAC1, VDAC3, TOMM20, HK1, and MFN2 primary ubiquitylation (Figures 3F–3J). Finally, consistent with the feedforward mechanism underlying accumulation of pS65-Ub (Harper et al., 2018; Pickrell and Youle, 2015; Yamano et al., 2016), all three UbVs blocked the accumulation of pS65-Ub on mitochondria, to levels similar to that found in PINK1^{-/-} or PARKIN^{C431S}-expressing cells (Figure 3K), and likewise blocked depolarization-dependent PARKIN recruitment to mitochondria, as examined by immunofluorescence (Figure S3J). Taken together, these data define a set of inhibitory UbVs for PARKIN and demonstrate that overall the Pt-PRM platform can be used to quantify the

Figure 3. Pt-PRM Allows Quantitative Analysis of Pathway Activators and Inhibitors

(A–C) The indicated HeLa PARKIN Flip-In T-REx cells were incubated with 50 μ M kinetin prior to depolarization (AO, 1 hr). Cell extracts (A) were analyzed by immunoblotting. Purified mitochondria (B and C) were analyzed by Pt-PRM. Error bars (B and C) represent SEM (n = 3). n.d., not determined.

(D) HeLa PARKIN Flip-In T-REx cells expressing UbVs targeting PARKIN were depolarized with AO (1 hr), and ubiquitylated proteins from mitochondria were immunoblotted with the indicated antibodies.

(E) UbV-expressing HeLa PARKIN Flip-In T-REx cells were depolarized (1 or 4 hr), and ubiquitylated proteins from mitochondria were subjected to Pt-PRM to quantify Ub chain linkages. Error bars represent SEM (n = 3). n.d., not determined.

(F–J) Pt-PRM analysis of PARKIN substrates VDAC1 (F), VDAC3 (G), TOMM20 (H), HK1 (I), and MFN2 (J) for cells from (E). Error bars represent SEM (n = 3).

(K) UbV-expressing HeLa PARKIN Flip-In T-REx cells were depolarized (1 hr) prior to the analysis of pS65-Ub using Pt-PRM. Error bars represent SEM (n = 3). See also Figure S3.

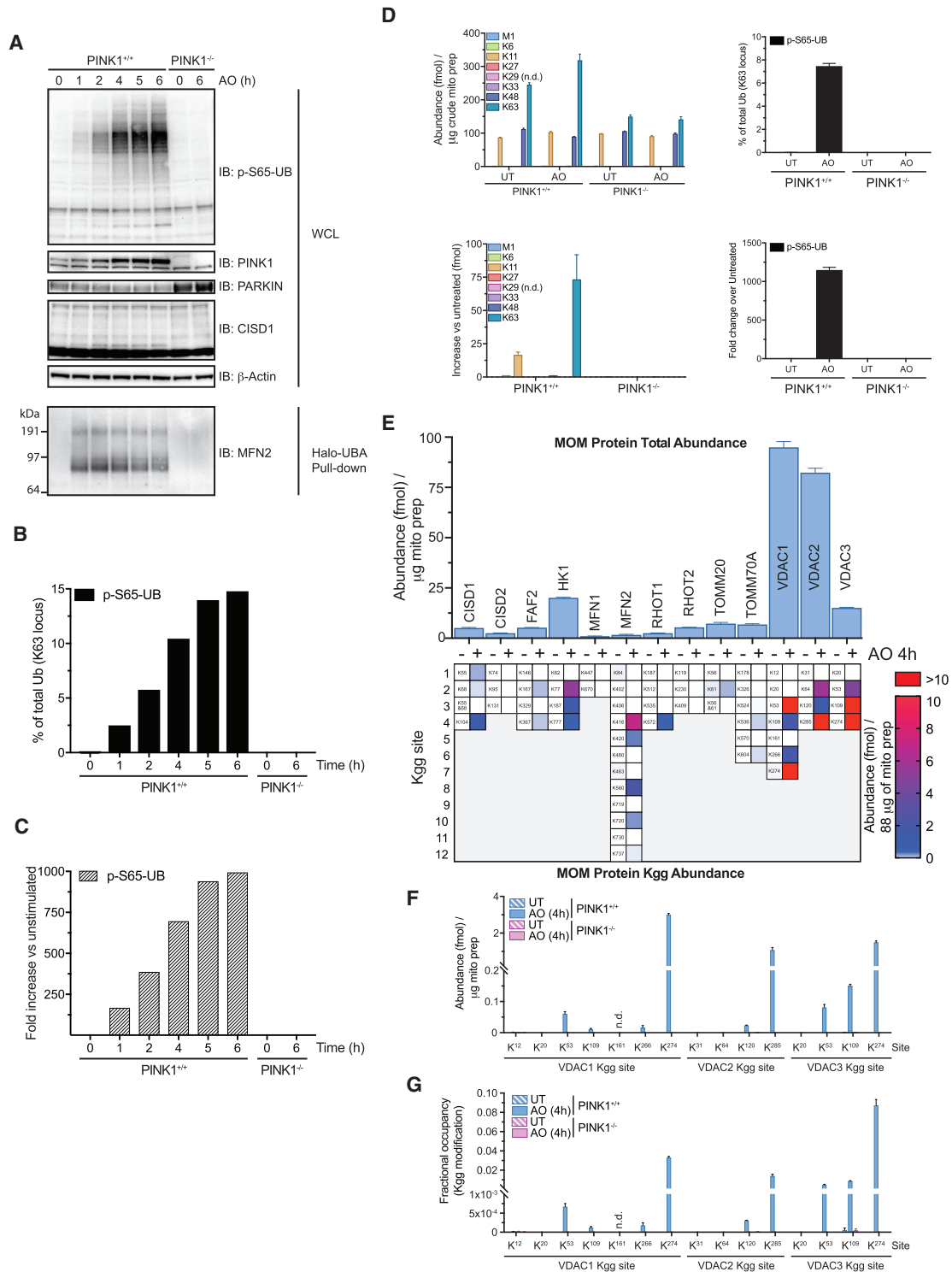


Figure 4. Quantitative Analysis of PINK1-PARKIN-Dependent MOM Ubiquitylation in NGN2-Induced Neurons

(A) ESCs were differentiated via NGN2 prior to depolarization with AO. Cell extracts were analyzed by immunoblotting or used for Ub enrichment prior to immunoblotting.

(B and C) Cell extracts from (A) were enriched for ubiquitylated proteins prior to Pt-PRM to quantify pS65-Ub. Plotted as percent (B) or fold increase (C). n = 1.

(D) ESCs were depolarized with AO (4 hr) and purified mitochondria were subjected to Pt-PRM. Total abundance or fold increase for individual Ub chain linkage types or pS65-Ub phosphorylation is plotted. Error bars represent SEM (n = 3). n.d., not determined.

(legend continued on next page)

effect of pathway modulators on Ub chain assembly, Ub phosphorylation, and primary site ubiquitylation.

Digital Snapshot of PINK1 and PARKIN Signaling in hESC-Derived Neurons

Having demonstrated that Pt-PRM can provide snapshots of PARKIN activity in the HeLa cell system, we next sought to examine PARKIN activity in the context of neuronal cells, which is poorly understood. We initially employed ESCs, with or without deletion of PINK1, and we converted these cells to iNeurons known to express markers of excitatory cortical neurons (Zhang et al., 2013) (~90% differentiation; Figure S4A). Upon depolarization, pS65-Ub increased ~900-fold over a 6-hr time course, as measured by Pt-PRM and immunoblotting of whole-cell extracts, with a Ub phosphorylation stoichiometry of 0.14 (Figures 4A–4C). The rate of Ub phosphorylation was comparatively slower than that seen in HeLa cells (maximal at ~1 hr) (Ordureau et al., 2014), and the appearance of pS65-Ub correlated with the accumulation of PINK1 (Figure 4A). Ub phosphorylation was completely PINK1 dependent (Figures 4A–4C). Examination of purified mitochondria from iNeurons 4 hr after depolarization revealed an ~1,100-fold increase in pS65-Ub, with a phosphorylation stoichiometry of 0.075, and 70- and 14-fold increases in K63 and K11 Ub chain linkages, respectively (Figure 4D). While a 2-fold increase in K6 chain linkages was detected, this is a much smaller increase than that seen in the HeLa cell system (Cunningham et al., 2015; Ordureau et al., 2014, 2015) (Figure 4D).

To examine ubiquitylation target specificity in iNeurons, we purified mitochondria with or without depolarization (4 hr) and either performed Pt-PRM directly or enriched for ubiquitylated proteins prior to Pt-PRM. First, we found that the relative abundance of PARKIN targets in iNeurons was comparable to that seen in HeLa cells ($R^2 = 0.86$), notable exceptions being HK1 and VDAC2, which are much more abundant in iNeurons (Figures 4E and S4B). PARKIN target abundance was also confirmed using label-free analysis of crude mitochondria (Figures S4C and S4D). Second, we detected ubiquitylation of 27 Kgg sites in 10 substrates (Figure 4E). The pattern of ubiquitylation was similar to that seen in HeLa cells, with VDACS carrying the majority of Ub modification. However, the total abundance of Ub on these substrates was ~10-fold lower than that seen in HeLa cells, which reflects much higher PARKIN levels in the HeLa cell system (Figure S4F). Moreover, the abundance of Ub modification on HK1 was substantially higher than that seen in HeLa cells, possibly reflecting overall higher HK1 abundance in iNeurons (Figures 4E and S4E). We examined the site specificity of VDAC ubiquitylation in detail, finding preferential ubiquitylation of K53 and K274 in VDAC1; K265 in VDAC2; and K274, K109, and K53 in VDAC3 (Figures 4E and 4F). The fractional occupancy of VDAC ubiquitylation at the most abundant sites ranged from 0.02 to 0.08 (Figure 4G). As expected, PARKIN target ubiquitylation required PINK1 (Figures 4F and S4E). As in HeLa cells, the total

abundance of the 15 proteins examined was essentially unchanged 4 hr after depolarization (Figure S4G), indicating that turnover of these proteins is not a major feature of endogenous PARKIN-dependent MOM ubiquitylation in iNeurons under the conditions used.

PARKIN Pathway Analysis in ESC-Derived DA Neurons

PINK1 and PARKIN mutations are associated with early onset forms of Parkinson's disease, leading to a loss of DA neurons (Valente et al., 2004). We therefore examined PARKIN and PINK1 targets in wild-type (WT) and PARKIN^{-/-} ESC-derived DA neurons (~40% tyrosine hydroxylase [TH] positive) produced as neuronal spheroids after 40 days in culture (Rigamonti et al., 2016) (see the STAR Methods). As in iNeurons, depolarization led to the accumulation of pS65-Ub with a stoichiometry of 0.02 at 8 hr relative to total Ub (110-fold increase), and this increase was dramatically dependent upon PARKIN (~5-fold increase) measured by Pt-PRM, consistent with PARKIN-dependent Ub chain assembly for promoting Ub phosphorylation (Figure 5A). Comparable results were obtained in purified mitochondria (80 µg), with a stoichiometry of 0.013 and a 60-fold increase in pS65-Ub 4 hr after depolarization (Figures 5B and 5C). We detected K11, K48, and K63 Ub chain linkages basally in DA neurons independent of PARKIN expression, and, upon depolarization, we detected an increase only in K63 chains (Figures 5D and 5E). The abundance of PARKIN targets in mitochondria measured either by label-free or Pt-PRM proteomics was similar to that seen in iNeurons (Figures 5F and S5A–S5C). Although only small amounts of mitochondria were available for this analysis, we nevertheless detected ubiquitylation of VDACS, CISD1, HK1, MFN2, and RHOT1, with significant overlap in site specificity when compared with iNeurons (see the Discussion for an in-depth comparison) (Figures 5G and S5D). These data indicate that many of the ubiquitylation events initially identified in HeLa cells are also found in these neuronal systems and likely represent bona fide endogenous PARKIN targets in neuronal lineages.

PARKIN pS65 Phosphorylation Is Required for Feedforward Pathway Activation in iNeurons

Having developed the iNeuron system for endogenous PARKIN pathway analysis, we addressed the question of whether PARKIN S65 phosphorylation is required for pathway activation. While some studies in HeLa cells indicate that constitutive overexpression of PARKIN^{S65A} can promote the pathway (Kane et al., 2014; Koyano et al., 2014; Shiba-Fukushima et al., 2012), other studies using regulated PARKIN expression suggest that PARKIN S65 phosphorylation is required (Kazlauskaitė et al., 2015; Ordureau et al., 2014, 2015). We gene edited ESCs to create homozygous PARKIN^{S65A} mutant cells, and we converted these cells to iNeurons together with PARKIN^{-/-} and PINK1^{-/-} cells as controls (Figures S4A, S6A, and S6B). The abundances of wild-type and S65A PARKIN were similar in iNeurons,

(E) Pt-PRM analysis of mitochondria from NGN2-derived neurons 4 hr post-depolarization after enrichment of ubiquitylated proteins or analysis of total PARKIN substrate abundance in enriched mitochondria. Error bars represent SEM (n = 3).

(F and G) Abundance (F) and fractional occupancy (G) of VDAC ubiquitylation in samples from (E). Error bars represent SEM (n = 3). n.d., not determined. See also Figure S4.

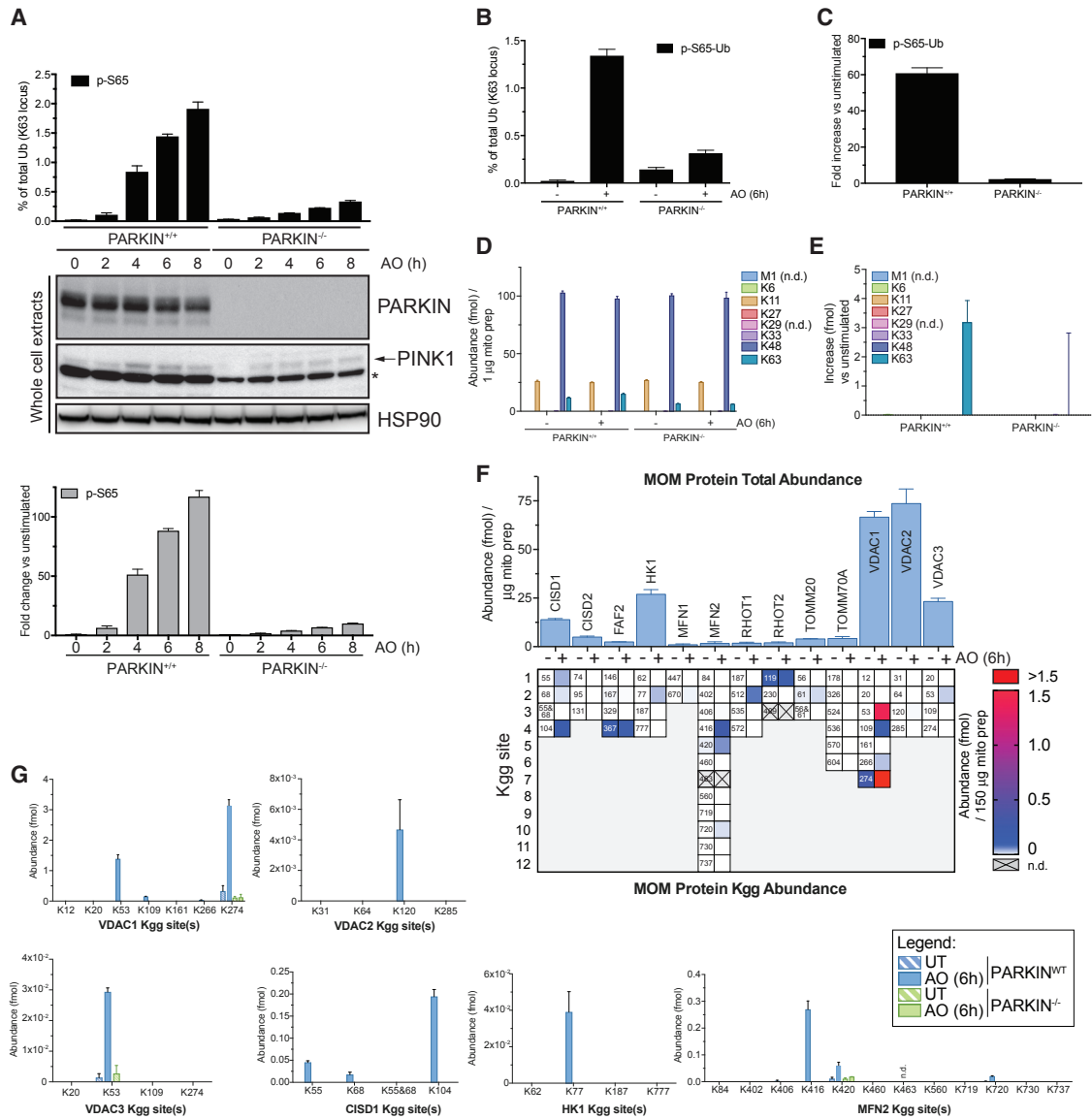


Figure 5. PARKIN Pathway Activation in Dopaminergic Neurons

(A) The indicated DA neurons 40 days post-differentiation from HUES1 cells (see the STAR Methods) were depolarized prior to analysis of cell extracts by Pt-PRM proteomics or immunoblotting. Error bars represent SEM (n = 2).

(B–E) Pt-PRM was performed on mitochondria isolated from cells described in (A) 6 hr post-depolarization to measure pS65-Ub (B and C) or Ub chain linkages (D and E). Error bars represent SEM (n = 3). n.d., not determined.

(F and G) PARKIN target ubiquitylation in purified mitochondria from DA neurons 40 days post-differentiation and 6 hr post-depolarization. The abundance of PARKIN targets in DA neurons as determined using Pt-PRM is shown (F, top). Heat map representation is shown (F, bottom) and individual plots (G). Error bars represent SEM (n = 3). n.d., not determined.

See also Figure S5.

indicating that the mutation doesn't destabilize PARKIN (Figure 6A). However, PARKIN^{S65A} cells were as defective in the accumulation of pS65-Ub as PARKIN^{-/-} cells, as measured by immunoblotting of whole-cell extracts over an 8-hr time course, despite comparable levels of PINK1 accumulation during the time course (Figure 6A). We then used purified mitochondria from cells 4 hr post-depolarization for Pt-PRM and immunoblotting, revealing reduced levels of pS65-Ub in PARKIN^{S65A} and

PARKIN^{-/-} iNeurons relative to that seen in PARKIN^{WT} iNeurons (Figures 6B and S6C). The finding that the addition of pS65-Ub to PARKIN^{S65A} *in vitro* can partially activate PARKIN's Ub ligase activity (Ordureau et al., 2014) together with the finding that PARKIN^{S65A} overexpression promotes the pathway (Kane et al., 2014; Koyano et al., 2014; Shiba-Fukushima et al., 2012) has led to the idea that pS65-Ub accumulation is the key step in PARKIN recruitment and activation. In addition, PARKIN

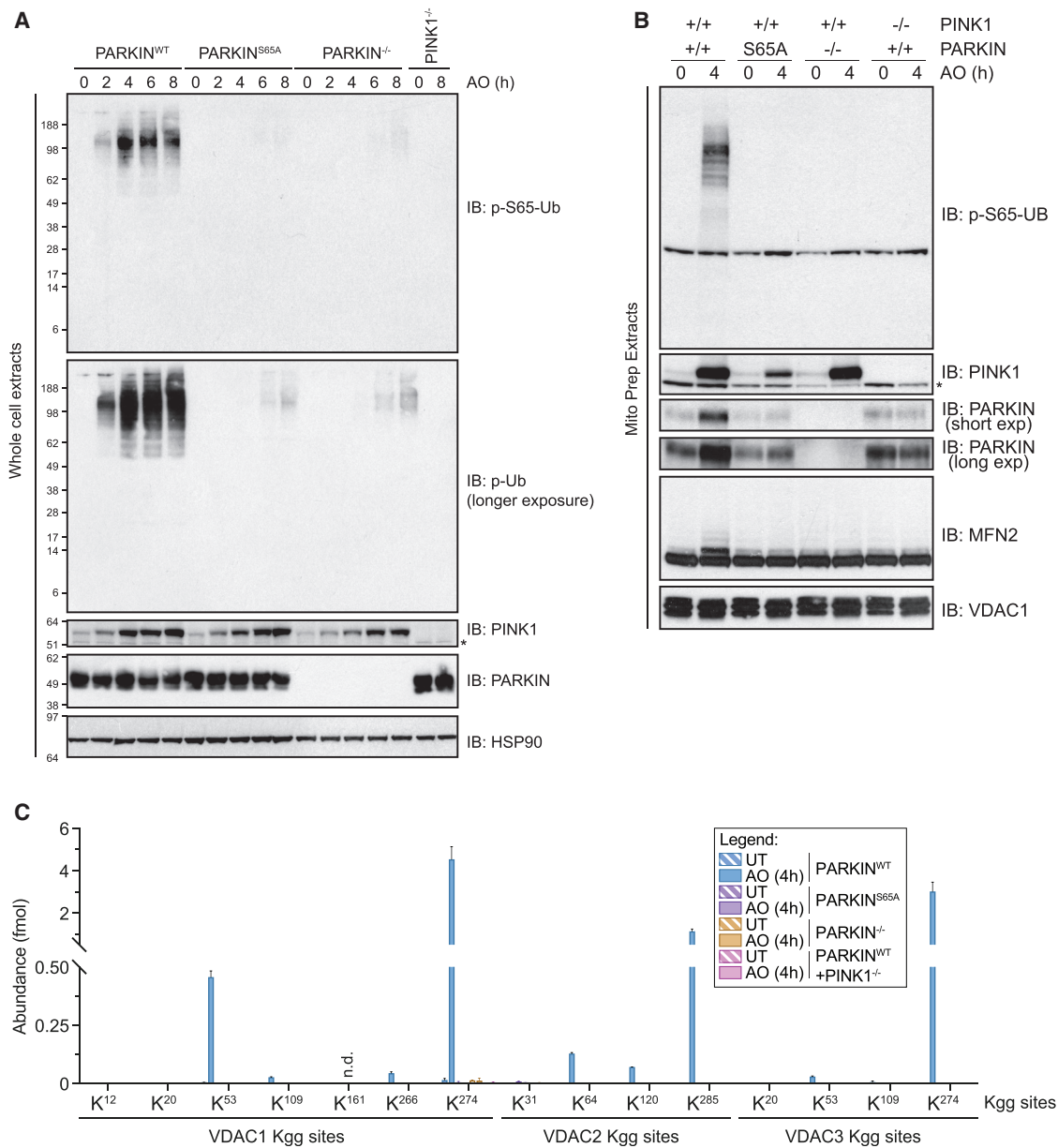


Figure 6. S65 in PARKIN's UBL Is Required for Pathway Activation in iNeurons

(A) The indicated ESCs were differentiated to iNeurons with NGN2 (8 days) prior to depolarization with AO. Cell extracts were immunoblotted with the indicated antibodies.

(B) Purified mitochondria from the indicated ESCs were immunoblotted with the indicated antibodies.

(C) Site-specific ubiquitylation of VDAC proteins in purified mitochondria from the indicated iNeurons 8 days post-differentiation and 4 hr post-depolarization. Error bars represent SEM (n = 3). n.d., not determined.

See also Figure S6.

mutants that cannot bind pS65-Ub are also defective in recruitment and activation (Kazlauskaitė et al., 2015; Wauer et al., 2015a), as we have also found by monitoring ubiquitylation of MFN2 and CISD1 in the context of PARKIN H302A and K151E mutants that do not bind pS65-Ub (Figure S6D). However, we found that, unlike PARKIN^{WT}, PARKIN^{S65A} was not enriched in purified mitochondria at 4 hr post-depolarization, despite the

presence of residual pS65-Ub (Figures 6A, 6B, and S6C). Moreover, ubiquitylation of primary PARKIN targets was not detected in PARKIN^{S65A}-expressing cells by both Pt-PRM or by immunoblotting for MFN2 (Figures 6B, 6C, and S6E). These data indicate a critical role for endogenous PARKIN S65 phosphorylation in promoting PARKIN E3 Ub ligase activity and the feedforward process (see the Discussion).

Stoichiometry of Ub Chain Phosphorylation by PINK1 Is Optimized for Mitophagy Receptor Recruitment

We next used Pt-PRM to address the role of Ub phosphorylation in mitophagy receptor recruitment. Artificial recruitment of overexpressed PINK1 to the MOM together with pull-down experiments using overexpressed Ub^{S65E} as a possible pS65-Ub mimetic led to the conclusion that phosphorylation itself on S65 of Ub chains on the MOM is directly responsible for recruitment of Ub chain-binding mitophagy receptors (OPTN, NDP52, TAX1BP1, and SQSTM1), in a manner that is PARKIN independent but relies on overexpressed PINK1's ability to phosphorylate pre-existing mitochondrial Ub (Lazarou et al., 2015). However, other studies suggested that endogenous levels of PINK1 are insufficient to support autophagy receptor recruitment and mitophagy and that pS65-Ub is actually inhibitory to receptor interaction *in vitro* (Heo et al., 2015; Richter et al., 2016). In addition, our previous tandem mass tagging (TMT)-based quantitative proteomics data (Rose et al., 2016) indicated enrichment of OPTN, NDP52 (CALCOCO2), NBR1, and p62 in purified mitochondria of cells expressing PARKIN^{WT}, but not in cells expressing PARKIN^{S65A}, despite residual pS65-Ub under this circumstance (Figure S7A).

To quantitatively examine the impact of Ub phosphorylation and chain assembly on mitophagy receptor recruitment and PARKIN activity on the MOM, we employed the HeLa system described above with or without constitutive overexpression of PINK1 at ~5-fold above endogenous under basal conditions, as measured by TMT-based proteomics (Figures 7A–7D). As outlined in Figure S7B, we then either left cells untreated or depolarized for 1 hr, isolated mitochondria, and analyzed pathway components using immunoblotting (Figure 7A); Pt-PRM to measure pS65-Ub, Ub chain linkages, and substrate's primary ubiquitylation (Figures 7B, 7C, 7E, and S7C–S7I); or TMT proteomics to quantify mitophagy receptor recruitment to mitochondria (Figure 7D). As expected, depolarization in the context of PARKIN^{WT} (but not PARKIN^{C431S} or PARKIN^{S65A}) cells with endogenous PINK1 induced robust formation of pS65-Ub (Figure 7A), with a stoichiometry of ~0.2 in purified mitochondria (Figure 7B) (Kane et al., 2014; Kazlauskaitė et al., 2014b; Koyano et al., 2014; Ordureau et al., 2014). In depolarized cells overexpressing PINK1 (~15-fold by TMT proteomics), we observed an increase in pS65-Ub stoichiometry on purified mitochondria to 0.65, and the stoichiometry of phosphorylation was only slightly reduced (0.55) in the context of C341S or S65A PARKIN, despite the

absence of PARKIN-dependent chain assembly (Figures 7A, 7B, and 7D). Importantly, this increase in pS65-Ub had no effect on the chain linkage types that were assembled upon PARKIN activation (Figure 7C). Thus, overexpressed PINK1 is capable of dramatically increasing the abundance of pS65-Ub chains on mitochondria with or without PARKIN activity.

In contrast with expectations if pS65-Ub is the direct recognition element for autophagy receptors, we found that OPTN, NDP52, and TAX1BP1 (and their ubiquitylated forms) were efficiently enriched in purified mitochondria when the pS65-Ub stoichiometry was ~0.2, but not when the stoichiometry was 0.65, as measured by either immunoblotting or TMT proteomics (Figures 7A and 7D). This is particularly striking in cells expressing inactive PARKIN and overexpressing PINK1, where only background levels of mitophagy receptors were detected despite a fractional occupancy for pS65-Ub of ~0.55 on mitochondria (Figures 7A–7D). In contrast, HSP90 or α -tubulin were not enriched in mitochondria under any condition examined, indicating specificity for autophagy receptor recruitment.

The finding that pS65-Ub can bind and activate PARKIN^{S65A} Ub ligase activity *in vitro* by ~900-fold (Ordureau et al., 2014) predicts that activation of this PARKIN mutant on the mitochondrial surface by pS65-Ub produced by PINK1 overexpression would promote primary target ubiquitylation. While strong ubiquitylation of VDACS and other PARKIN targets was observed with endogenous PINK1, target ubiquitylation was largely absent in the context of PARKIN^{S65A} with either endogenous or overexpressed PINK1, despite the presence of abundant pS65-Ub (Figures 7E and S7C–S7I). These results have implications for the mechanism by which PARKIN and Ub phosphorylation by PINK1 promotes PARKIN retention on the MOM (see the Discussion).

DISCUSSION

Comprehensive measurement of the dynamics, specificity, stoichiometry, and spatial organization of Ub-driven signaling systems in cells represents a major challenge for the field. Here we develop digital snapshot proteomics to define the dynamics and site specificity for structurally diverse PARKIN targets on the MOM in neurons, and we use the system to mechanistically evaluate models for PARKIN activation and mitophagy receptor recruitment to the MOM (Figure 7F).

PARKIN activation leads to extensive ubiquitylation of numerous MOM proteins, but no clearly definable targeting

Figure 7. Ub Chain Hyper-phosphorylation on Mitochondria Is Inhibitory to Mitophagy Receptor Recruitment

(A) The indicated HeLa cells were left untreated or depolarized with AO (1 hr). Purified mitochondria from these cells were subjected to immunoblotting. HSP90 and α -tubulin found in low levels in crude mitochondria were used as controls for non-specific protein retention on the MOM.

(B) Pt-PRM was used to quantify pS65-Ub on enriched mitochondria from cells in (A). Error bars represent SEM (n = 3).

(C) Ub chain linkage analysis by Pt-PRM on enriched mitochondria from cells in (A). Increases in individual chain linkage types were normalized to VDAC1 abundance by Pt-PRM. Error bars represent SEM (n = 3). n.d., not determined.

(D) Mitochondria from cells in (A) were trypsinized, peptides from the indicated cell lines labeled individually with one of 10 TMT isobaric tags, and the mixture subjected to LC-MS³. Individual quantified peptides from relevant proteins were combined to determine relative abundance across each cell line and condition. "n" in each panel refers to the number of peptides quantified from the indicated protein used for quantification.

(E) Pt-PRM of VDAC1–3 primary ubiquitylation sites was measured on mitochondria from cells described in (A) after enrichment of ubiquitylated proteins. Error bars represent SEM (n = 3). n.d., not determined.

(F) Scheme illustrating the following: (1) lysine specificity within PARKIN's ubiquitylated targets on the MOM upon activation, and (2) the marked preference for mitophagy receptor (i.e., OPTN) recruitment to Ub chains with low-phosphorylation stoichiometry.

See also Figure S7.

elements such as degrons have been uncovered, leading to the idea that PARKIN may lack sequence or structural specificity (Harper et al., 2018; Pickrell and Youle, 2015; Sarraf et al., 2013; Yamano et al., 2016). The ability to quantitatively examine site specificity and stoichiometry within individual targets indicates a dramatic preference of PARKIN for particular surface Lys residues (Figure 7F). For example, K53 and K274 on cytosolic face of VDAC1 are dramatically preferred when compared kinetically with other cytosolic loop residues in the protein. Moreover, K12 and K20 on the N-terminal helix that extends into the β -barrel in solution structures of VDAC1 (Hiller et al., 2008) are largely immune to ubiquitylation (Figures 1A and 2C). There are several analogous examples across PARKIN targets, including FAF2, which is readily ubiquitylated on K167 and K367, but not detectably ubiquitylated on K146 or K329, consistent with relative quantification measured by Kgg-TMT proteomics for FAF2 (Rose et al., 2016). Interestingly, PARKIN displays specificity for individual nearby Lys residues within distinct structural environments, including helical elements such as those in MFN2 and loop elements such as in VDACS, and we found, for example, no clear evidence that accessible surface area contributes to Lys specificity based on structures of isolated target proteins. It is possible that higher-order protein assemblies or interactions with lipids in the MOM sterically block access of PARKIN to particular Lys residues, thereby contributing to the apparent specificity that we observed.

PARKIN and PINK1 mutants lead to a loss of DA neurons in PD patients, yet we know little about PARKIN targets in neurons. Using ESCs converted to iNeurons or DA neurons, we determined that PARKIN activity upon depolarization is detectable and quantifiable, and, moreover, it displays considerable overlap in target site specificity when compared with the frequently used HeLa cell model. First, in both neurons and HeLa cells, VDAC proteins are the most abundant substrates and carry the bulk of primary ubiquitylation observed. Within VDACS, the site specificity is very similar between the two systems, the exception being that K161 ubiquitylation in VDAC1 was not detected in neurons (Figures 4E–4G and S5D). This is potentially reflected in the low rate and amplitude of ubiquitylation of K161 in HeLa cells when compared with preferred sites (Figures 2C and 2D). There are conflicting reports in the literature, with evidence both for (Geisler et al., 2010) and against (Narendra et al., 2010a) VDAC involvement in PARKIN-dependent mitophagy, and therefore, further studies are necessary to understand the contribution of VDAC ubiquitylation to downstream signaling. Second, the site specificity for the majority of lower abundance PARKIN targets was quite similar overall between neurons and HeLa cells, with all 15 sites detected with 100 μ g Ub-enriched mitochondria from HeLa cells being found in iNeurons (Figure S5D). We did, however, find several differences in site preference. For example, K560 in MFN2 was ubiquitylated in iNeurons, but not in HeLa cells or DA neurons, while RHOT1 K512 and K572 were differentially modified in DA and iNeurons (Figure S5D). In addition, K167 and K367 in FAF2 were inducibly ubiquitylated in HeLa cells and iNeurons, but these sites were constitutively ubiquitylated in DA neurons and did not increase upon depolarization (Figure S5D). The biological relevance of these differences, if any, remains unknown, but we speculate that such al-

terations in specificity could reflect distinct interaction partners that affect access of PARKIN to particular Lys residues in the target protein. The primary differences between the systems are the magnitude of Ub primary site abundance and the more rapid accumulation of pS65-Ub accumulation in the HeLa system relative to neurons (Figures 2B, 4A, and 4E) (Ordureau et al., 2014). This likely reflects the much higher PARKIN levels in the HeLa cell system relative to neurons (Figure S4F).

PARKIN activation on damaged mitochondria involves multiple steps, including PINK1-dependent phosphorylation of S65 on both Ub linked to proteins on the MOM and PARKIN's UBL, and biochemical studies (Ordureau et al., 2015) indicate that the fully active form of PARKIN is both phosphorylated on its UBL and bound to pS65-Ub on the MOM (reviewed in Harper et al., 2018 and Yamano et al., 2016). Binding of pS65-Ub to unphosphorylated PARKIN greatly accelerates PARKIN UBL phosphorylation by PINK1 *in vitro* (Kazlauskaitė et al., 2015; Wauer et al., 2015a) (Figure S7J), suggesting that low levels of phosphorylation of pre-existing Ub on mitochondria, detectable in PARKIN^{-/-} neurons (Figures 5 and 6), could serve to initiate recruitment and activation of PARKIN from the cytosol. In contrast, PARKIN^{H302A} that cannot bind pS65-Ub is still detectably phosphorylated on its UBL (Kazlauskaitė et al., 2015; Pao et al., 2016), suggesting the possibility that PARKIN UBL phosphorylation on damaged mitochondria can occur independently of pS65-Ub binding (Harper et al., 2018; Yamano et al., 2016), albeit at a much lower rate in the absence of the feedforward mechanism.

To further understand the contribution of PARKIN UBL phosphorylation, we employed iNeurons from endogenous PARKIN^{S65A} hESCs, demonstrating that this PARKIN mutant cannot activate the feedforward ubiquitylation cascade, despite experiments that demonstrate activation of PARKIN^{S65A} ligase activity by binding to pS65-Ub *in vitro* (Ordureau et al., 2014). The Pt-PRM system also facilitates an analysis of the contribution of pS65-Ub accumulation on the MOM to the recruitment of mitophagy receptors. Accumulation of pS65-Ub on the MOM was dramatically reduced in PARKIN^{S65A} cells, consistent with the absence of new chain synthesis, and PARKIN^{S65A} was not enriched in damaged mitochondria, despite residual pS65-Ub (Figures 6B and S6C). Moreover, no primary site ubiquitylation was observed across all the PARKIN targets examined, indicating that PARKIN^{S65A} is unable to mount detectable activity on the MOM if even transiently bound to pS65-Ub. Previous biochemical studies indicate that PARKIN UBL phosphorylation greatly increases the affinity of PARKIN for pS65-Ub, from \sim 400 to \sim 20 nM (Ordureau et al., 2014; Sauvé et al., 2015). Thus, we speculate that phosphorylation of PARKIN's UBL both increases its affinity for pS65-Ub on the MOM, thereby specifying PARKIN retention, while also locking PARKIN in a catalytically active conformation, as indicated by the finding that simply phosphorylating PARKIN's UBL can increase Ub chain assembly activity by 2,500-fold (Ordureau et al., 2014). We hypothesize that these events constitute the PINK1-driven PARKIN feedforward mechanism.

K63-linked Ub chains are thought to function as the primary receptors for mitophagy adaptor proteins including OPTN, but the role of phosphorylation in receptor recruitment is unclear,

with evidence for and against a direct role of pS65-Ub in mitophagy receptor recruitment (Heo et al., 2015; Lazarou et al., 2015; Ordureau et al., 2015; Richter et al., 2016; reviewed in Harper et al., 2018 and Yamano et al., 2016). We employed Pt-PRM to quantitatively evaluate the influence of pS65-Ub stoichiometry on mitophagy receptor recruitment. In the HeLa cell system, endogenous PINK1 produces a fractional occupancy of ~ 0.2 on the MOM (Ordureau et al., 2014). We found that increasing the fractional occupancy to 0.55–0.65 by stable overexpression of PINK1 reduces the association of OPTN, p62, TAX1BP1, and NDP52, rather than increasing association, as would be expected if mitophagy receptors bound specifically to pS65-Ub within chains. The finding that PARKIN is highly active on the MOM, as measured by Pt-PRM under conditions where the fractional occupancy of Ub phosphorylation is ~ 0.2 , is consistent with a model in which PARKIN associates with pS65-Ub units within MOM-associated Ub chains and unphosphorylated units within these Ub chains would preferentially associate with mitophagy receptors (reviewed in Harper et al., 2018) (Figure 7F). Based on available data (reviewed in Behrends and Harper, 2011), dimeric UBAN domains in OPTN would interact individually with a unit of di-Ub K63 chains generated by PARKIN. In essence, the stoichiometry of Ub phosphorylation at endogenous PINK1 levels is optimized for promotion of both PARKIN recruitment via pS65-Ub units and mitophagy receptor recruitment via unphosphorylated Ub units within chains built by PARKIN (Figure 7F). We also note that PARKIN's ability to ubiquitylate primary targets is reduced in the context of PINK1 overexpression (Figure 7). The basis for this is unclear at present. This model is also supported by recent structural data indicating that, in di-Ub, pS65 in neither the proximal nor distal Ub is nearby the UBAN domain in OPTN, which is inconsistent with a direct positive role of Ub phosphorylation in OPTN recruitment (Li et al., 2018).

The fate of PARKIN targets on the MOM is unclear. While some ubiquitylated proteins are apparently employed for mitophagy receptor binding, some studies have suggested that several PARKIN substrates are degraded by the proteasome in cells overexpressing PARKIN (Chan et al., 2011; Geisler et al., 2010; Tanaka et al., 2010). The use of Pt-PRM to quantify target protein abundance overcomes the limitation of immunoblots for examination of the abundance of ubiquitylated proteins. We find in both HeLa cells and in neurons that the abundance of the PARKIN targets examined here are not appreciably reduced at 1 or 4 hr after depolarization, respectively. It is possible that overexpression of PARKIN can produce sufficient K11 and/or K48-Ub chains on PARKIN targets to support extraction by p97 and delivery to the proteasome (Chan et al., 2011; Geisler et al., 2010; Tanaka et al., 2010), but our chain linkage analysis suggests little K48 chain production in neurons with endogenous levels of PARKIN. This is also consistent with the previous finding that K63 chains contribute substantially to mitophagy induced by PARKIN (Cunningham et al., 2015; Ordureau et al., 2014, 2015). Interestingly, induced neurons employed here had relatively lower levels of K6 Ub chains upon depolarization than HeLa cells overexpressing PARKIN. Given that mitochondrially localized USP30 prefers to disassemble K6 chains (Cunningham et al., 2015; Gersch et al., 2017; Wauer et al., 2015b), we speculate

that the lower relative levels of this chain linkage in induced neurons could reflect USP30 activity.

In conclusion, this work now sets the stage for further dissection of the biochemical mechanisms underlying PARKIN function in neuronal systems, and also it suggests that analogous proteomic approaches may be useful in uncovering the biochemical mechanisms of other pathway defects in neurodegenerative disease more generally.

STAR★METHODS

Detailed methods are provided in the online version of this paper and include the following:

- KEY RESOURCES TABLE
- STAR METHOD DETAILS
 - Cell culture, immunoblotting, and mitochondrial protein isolation
 - Mitochondrial poly-ubiquitin capture and proteomics
 - Heavy reference peptides and characterization
 - Proteomics – Label-free Analysis
 - Proteomics – TMT Quantification
 - Comparison of pS65-Ub and Ub chain linkages in crude versus sucrose density gradient purified mitochondria
 - Gene-Editing and differentiation
 - Mitophagy assays
 - Selection of UbVs for PARKIN
 - ELISA to evaluate UbV binding and specificity
 - Analysis of UbV activity *in vitro* and *in vivo*
 - Analysis of Kinetin activity *in vivo*
 - Structural modeling
- QUANTIFICATION AND STATISTICAL ANALYSIS
- CONTACT FOR REAGENT AND RESOURCE SHARING

SUPPLEMENTAL INFORMATION

Supplemental Information includes seven figures, two tables, and two data files and can be found with this article online at <https://doi.org/10.1016/j.molcel.2018.03.012>.

ACKNOWLEDGMENTS

We thank Nick Hertz (Stanford University) for discussions and advice on the use of mitokinin. This work was supported by the NIH (R37 NS083524 and RO1 GM095567 to J.W.H., RO1 GM067945 to S.P.G., and K01DK098285 to J.A.P.), the Michael J. Fox Foundation (11115.01 to J.W.H.), an Edward R. and Anne G. Lefler Center Postdoctoral Fellowship (A.O.), a Sara Elizabeth O'Brien Trust Postdoctoral Fellowship (J.-M.H.), a Cancer Research Society/BMO Bank of Montreal Scholarship for the Next Generation of Scientists (W.Z.), a Genome Canada Disruptive Innovation in Genomics grant (OGI-119 to S.S.S.), the Harvard Medical School Cell Biology Initiative for Molecular Trafficking and Neurodegeneration, and a generous gift from Ned Goodnow (J.W.H.).

AUTHOR CONTRIBUTIONS

A.O. and J.W.H. conceived the study. A.O. created cell lines, performed proteomics, and performed all biochemical assays. W.Z. identified UbVs under the direction of S.S.S. J.-M.H. made cell lines. J.Z., E.F.C., Z.H., and T.A. performed gene editing and neuronal differentiation. L.L.R. directed the

production of DA neurons by T.A. J.A.P. and S.P.G. provided proteomics expertise. J.W.H. and A.O. wrote the paper with input from all authors.

DECLARATION OF INTERESTS

J.W.H. is a consultant for SV Brahma Discovery, which includes the topic of selective autophagy.

Received: November 27, 2017

Revised: February 21, 2018

Accepted: March 8, 2018

Published: April 12, 2018

REFERENCES

- Behrends, C., and Harper, J.W. (2011). Constructing and decoding unconventional ubiquitin chains. *Nat. Struct. Mol. Biol.* *18*, 520–528.
- Bingol, B., Tea, J.S., Phu, L., Reichelt, M., Bakalarski, C.E., Song, Q., Foreman, O., Kirkpatrick, D.S., and Sheng, M. (2014). The mitochondrial deubiquitinase USP30 opposes parkin-mediated mitophagy. *Nature* *510*, 370–375.
- Calvo, S.E., Clauser, K.R., and Mootha, V.K. (2016). MitoCarta2.0: an updated inventory of mammalian mitochondrial proteins. *Nucleic Acids Res.* *44* (D1), D1251–D1257.
- Chan, N.C., Salazar, A.M., Pham, A.H., Sweredoski, M.J., Kolawa, N.J., Graham, R.L., Hess, S., and Chan, D.C. (2011). Broad activation of the ubiquitin-proteasome system by Parkin is critical for mitophagy. *Hum. Mol. Genet.* *20*, 1726–1737.
- Chen, G., Gulbranson, D.R., Hou, Z., Bolin, J.M., Ruotti, V., Probasco, M.D., Smuga-Otto, K., Howden, S.E., Diol, N.R., Propson, N.E., et al. (2011). Chemically defined conditions for human iPSC derivation and culture. *Nat. Methods* *8*, 424–429.
- Cowan, C.A., Klimanskaya, I., McMahon, J., Atienza, J., Witmyer, J., Zucker, J.P., Wang, S., Morton, C.C., McMahon, A.P., Powers, D., and Melton, D.A. (2004). Derivation of embryonic stem-cell lines from human blastocysts. *N. Engl. J. Med.* *350*, 1353–1356.
- Cunningham, C.N., Baughman, J.M., Phu, L., Tea, J.S., Yu, C., Coons, M., Kirkpatrick, D.S., Bingol, B., and Corn, J.E. (2015). USP30 and parkin homeostatically regulate atypical ubiquitin chains on mitochondria. *Nat. Cell Biol.* *17*, 160–169.
- Eng, J.K., McCormack, A.L., and Yates, J.R. (1994). An approach to correlate tandem mass spectral data of peptides with amino acid sequences in a protein database. *J. Am. Soc. Mass. Spectrom.* *5*, 976–989.
- Ernst, A., Avvakumov, G., Tong, J., Fan, Y., Zhao, Y., Alberts, P., Persaud, A., Walker, J.R., Neculai, A.M., Neculai, D., et al. (2013). A strategy for modulation of enzymes in the ubiquitin system. *Science* *339*, 590–595.
- Fiesel, F.C., Caulfield, T.R., Moussaud-Lamodière, E.L., Ogaki, K., Dourado, D.F., Flores, S.C., Ross, O.A., and Springer, W. (2015). Structural and Functional Impact of Parkinson Disease-Associated Mutations in the E3 Ubiquitin Ligase Parkin. *Hum. Mutat.* *36*, 774–786.
- Geisler, S., Holmström, K.M., Skujat, D., Fiesel, F.C., Rothfuss, O.C., Kahle, P.J., and Springer, W. (2010). PINK1/Parkin-mediated mitophagy is dependent on VDAC1 and p62/SQSTM1. *Nat. Cell Biol.* *12*, 119–131.
- Gersch, M., Gladkova, C., Schubert, A.F., Michel, M.A., Maslen, S., and Komander, D. (2017). Mechanism and regulation of the Lys6-selective deubiquitinase USP30. *Nat. Struct. Mol. Biol.* *24*, 920–930.
- Harper, J.W., Ordureau, A., and Heo, J.M. (2018). Building and decoding ubiquitin chains for mitophagy. *Nat. Rev. Mol. Cell Biol.* *19*, 93–108.
- Heo, J.M., Ordureau, A., Paulo, J.A., Rinehart, J., and Harper, J.W. (2015). The PINK1-PARKIN Mitochondrial Ubiquitylation Pathway Drives a Program of OPTN/NDP52 Recruitment and TBK1 Activation to Promote Mitophagy. *Mol. Cell* *60*, 7–20.
- Hertz, N.T., Berthet, A., Sos, M.L., Thorn, K.S., Burlingame, A.L., Nakamura, K., and Shokat, K.M. (2013). A neo-substrate that amplifies catalytic activity of parkinson's-disease-related kinase PINK1. *Cell* *154*, 737–747.
- Hiller, S., Garces, R.G., Malia, T.J., Orekhov, V.Y., Colombini, M., and Wagner, G. (2008). Solution structure of the integral human membrane protein VDAC-1 in detergent micelles. *Science* *321*, 1206–1210.
- Hung, V., Lam, S.S., Udeshi, N.D., Svinkina, T., Guzman, G., Mootha, V.K., Carr, S.A., and Ting, A.Y. (2017). Proteomic mapping of cytosol-facing outer mitochondrial and ER membranes in living human cells by proximity biotinylation. *eLife* *6*, 1206.
- Hunter, T. (2007). The age of crosstalk: phosphorylation, ubiquitination, and beyond. *Mol. Cell* *28*, 730–738.
- Huttlin, E.L., Jedrychowski, M.P., Elias, J.E., Goswami, T., Rad, R., Beausoleil, S.A., Villen, J., Haas, W., Sowa, M.E., and Gygi, S.P. (2010). A tissue-specific atlas of mouse protein phosphorylation and expression. *Cell* *143*, 1174–1189.
- Kane, L.A., Lazarou, M., Fogel, A.I., Li, Y., Yamano, K., Sarraf, S.A., Banerjee, S., and Youle, R.J. (2014). PINK1 phosphorylates ubiquitin to activate Parkin E3 ubiquitin ligase activity. *J. Cell Biol.* *205*, 143–153.
- Kazlauskaitė, A., Kelly, V., Johnson, C., Baillie, C., Hastie, C.J., Peggie, M., Macartney, T., Woodroof, H.I., Alessi, D.R., Pedrioli, P.G., and Muqit, M.M. (2014a). Phosphorylation of Parkin at Serine65 is essential for activation: elaboration of a Miro1 substrate-based assay of Parkin E3 ligase activity. *Open Biol.* *4*, 130213.
- Kazlauskaitė, A., Kondapalli, C., Gourlay, R., Campbell, D.G., Ritorto, M.S., Hofmann, K., Alessi, D.R., Knebel, A., Trost, M., and Muqit, M.M. (2014b). Parkin is activated by PINK1-dependent phosphorylation of ubiquitin at Ser65. *Biochem. J.* *460*, 127–139.
- Kazlauskaitė, A., Martínez-Torres, R.J., Wilkie, S., Kumar, A., Peltier, J., Gonzalez, A., Johnson, C., Zhang, J., Hope, A.G., Peggie, M., et al. (2015). Binding to serine 65-phosphorylated ubiquitin primes Parkin for optimal PINK1-dependent phosphorylation and activation. *EMBO Rep.* *16*, 939–954.
- Koyano, F., Okatsu, K., Kosako, H., Tamura, Y., Go, E., Kimura, M., Kimura, Y., Tsuchiya, H., Yoshihara, H., Hirokawa, T., et al. (2014). Ubiquitin is phosphorylated by PINK1 to activate parkin. *Nature* *510*, 162–166.
- Kulathu, Y., and Komander, D. (2012). Atypical ubiquitylation - the unexplored world of polyubiquitin beyond Lys48 and Lys63 linkages. *Nat. Rev. Mol. Cell Biol.* *13*, 508–523.
- Lazarou, M., Jin, S.M., Kane, L.A., and Youle, R.J. (2012). Role of PINK1 binding to the TOM complex and alternate intracellular membranes in recruitment and activation of the E3 ligase Parkin. *Dev. Cell* *22*, 320–333.
- Lazarou, M., Narendra, D.P., Jin, S.M., Tekle, E., Banerjee, S., and Youle, R.J. (2013). PINK1 drives Parkin self-association and HECT-like E3 activity upstream of mitochondrial binding. *J. Cell Biol.* *200*, 163–172.
- Lazarou, M., Sliter, D.A., Kane, L.A., Sarraf, S.A., Wang, C., Burman, J.L., Sideris, D.P., Fogel, A.I., and Youle, R.J. (2015). The ubiquitin kinase PINK1 recruits autophagy receptors to induce mitophagy. *Nature* *524*, 309–314.
- Li, F., Xu, D., Wang, Y., Zhou, Z., Liu, J., Hu, S., Gong, Y., Yuan, J., and Pan, L. (2018). Structural insights into the ubiquitin recognition by OPTN (optineurin) and its regulation by TBK1-mediated phosphorylation. *Autophagy* *14*, 66–79.
- MacLean, B., Tomazela, D.M., Shulman, N., Chambers, M., Finney, G.L., Frewen, B., Kern, R., Tabb, D.L., Liebler, D.C., and MacCoss, M.J. (2010). Skyline: an open source document editor for creating and analyzing targeted proteomics experiments. *Bioinformatics* *26*, 966–968.
- McAlister, G.C., Huttlin, E.L., Haas, W., Ting, L., Jedrychowski, M.P., Rogers, J.C., Kuhn, K., Pike, I., Grothe, R.A., Blethrow, J.D., and Gygi, S.P. (2012). Increasing the multiplexing capacity of TMTs using reporter ion isotopologues with isobaric masses. *Anal. Chem.* *84*, 7469–7478.
- McAlister, G.C., Nusinow, D.P., Jedrychowski, M.P., Wühr, M., Huttlin, E.L., Erickson, B.K., Rad, R., Haas, W., and Gygi, S.P. (2014). MultiNotch MS3 enables accurate, sensitive, and multiplexed detection of differential expression across cancer cell line proteomes. *Anal. Chem.* *86*, 7150–7158.
- Narendra, D., Tanaka, A., Suen, D.F., and Youle, R.J. (2008). Parkin is recruited selectively to impaired mitochondria and promotes their autophagy. *J. Cell Biol.* *183*, 795–803.

- Narendra, D., Kane, L.A., Hauser, D.N., Fearnley, I.M., and Youle, R.J. (2010a). p62/SQSTM1 is required for Parkin-induced mitochondrial clustering but not mitophagy; VDAC1 is dispensable for both. *Autophagy* 6, 1090–1106.
- Narendra, D.P., Jin, S.M., Tanaka, A., Suen, D.F., Gautier, C.A., Shen, J., Cookson, M.R., and Youle, R.J. (2010b). PINK1 is selectively stabilized on impaired mitochondria to activate Parkin. *PLoS Biol.* 8, e1000298.
- Okatsu, K., Koyano, F., Kimura, M., Kosako, H., Saeki, Y., Tanaka, K., and Matsuda, N. (2015). Phosphorylated ubiquitin chain is the genuine Parkin receptor. *J. Cell Biol.* 209, 111–128.
- Ordureau, A., Sarraf, S.A., Duda, D.M., Heo, J.M., Jedrychowski, M.P., Sviderskiy, V.O., Olszewski, J.L., Koerber, J.T., Xie, T., Beausoleil, S.A., et al. (2014). Quantitative proteomics reveal a feedforward mechanism for mitochondrial PARKIN translocation and ubiquitin chain synthesis. *Mol. Cell* 56, 360–375.
- Ordureau, A., Heo, J.M., Duda, D.M., Paulo, J.A., Olszewski, J.L., Yanishevski, D., Rinehart, J., Schulman, B.A., and Harper, J.W. (2015). Defining roles of PARKIN and ubiquitin phosphorylation by PINK1 in mitochondrial quality control using a ubiquitin replacement strategy. *Proc. Natl. Acad. Sci. USA* 112, 6637–6642.
- Pao, K.C., Stanley, M., Han, C., Lai, Y.C., Murphy, P., Balk, K., Wood, N.T., Corti, O., Corvol, J.C., Muqit, M.M., and Virdee, S. (2016). Probes of ubiquitin E3 ligases enable systematic dissection of parkin activation. *Nat. Chem. Biol.* 12, 324–331.
- Phu, L., Izrael-Tomasevic, A., Matsumoto, M.L., Bustos, D., Dynek, J.N., Fedorova, A.V., Bakalarski, C.E., Arnott, D., Deshayes, K., Dixit, V.M., et al. (2011). Improved quantitative mass spectrometry methods for characterizing complex ubiquitin signals. *Mol. Cell. Proteomics* 10, M110.003756.
- Pickrell, A.M., and Youle, R.J. (2015). The roles of PINK1, parkin, and mitochondrial fidelity in Parkinson's disease. *Neuron* 85, 257–273.
- Richter, B., Sliter, D.A., Herhaus, L., Stolz, A., Wang, C., Beli, P., Zaffagnini, G., Wild, P., Martens, S., Wagner, S.A., et al. (2016). Phosphorylation of OPTN by TBK1 enhances its binding to Ub chains and promotes selective autophagy of damaged mitochondria. *Proc. Natl. Acad. Sci. USA* 113, 4039–4044.
- Rigamonti, A., Repetti, G.G., Sun, C., Price, F.D., Reny, D.C., Rapino, F., Weisinger, K., Benkler, C., Peterson, Q.P., Davidow, L.S., et al. (2016). Large-Scale Production of Mature Neurons from Human Pluripotent Stem Cells in a Three-Dimensional Suspension Culture System. *Stem Cell Reports* 6, 993–1008.
- Rose, C.M., Isasa, M., Ordureau, A., Prado, M.A., Beausoleil, S.A., Jedrychowski, M.P., Finley, D.J., Harper, J.W., and Gygi, S.P. (2016). Highly Multiplexed Quantitative Mass Spectrometry Analysis of Ubiquitylomes. *Cell Syst.* 3, 395–403.e4.
- Rual, J.F., Hirozane-Kishikawa, T., Hao, T., Bertin, N., Li, S., Dricot, A., Li, N., Rosenberg, J., Lamesch, P., Vidalain, P.O., et al. (2004). Human ORFome version 1.1: a platform for reverse proteomics. *Genome Res.* 14 (10B), 2128–2135.
- Sarraf, S.A., Raman, M., Guarani-Pereira, V., Sowa, M.E., Huttlin, E.L., Gygi, S.P., and Harper, J.W. (2013). Landscape of the PARKIN-dependent ubiquitylome in response to mitochondrial depolarization. *Nature* 496, 372–376.
- Sauvé, V., Lilov, A., Seirafi, M., Vranas, M., Rasool, S., Kozlov, G., Sprules, T., Wang, J., Trempe, J.F., and Gehring, K. (2015). A Ubl/ubiquitin switch in the activation of Parkin. *EMBO J.* 34, 2492–2505.
- Shiba-Fukushima, K., Imai, Y., Yoshida, S., Ishihama, Y., Kanao, T., Sato, S., and Hattori, N. (2012). PINK1-mediated phosphorylation of the Parkin ubiquitin-like domain primes mitochondrial translocation of Parkin and regulates mitophagy. *Sci. Rep.* 2, 1002.
- Tanaka, A., Cleland, M.M., Xu, S., Narendra, D.P., Suen, D.F., Karbowski, M., and Youle, R.J. (2010). Proteasome and p97 mediate mitophagy and degradation of mitofusins induced by Parkin. *J. Cell Biol.* 191, 1367–1380.
- Tonikian, R., Zhang, Y., Boone, C., and Sidhu, S.S. (2007). Identifying specificity profiles for peptide recognition modules from phage-displayed peptide libraries. *Nat. Protoc.* 2, 1368–1386.
- Tyanova, S., Temu, T., Sinitcyn, P., Carlson, A., Hein, M.Y., Geiger, T., Mann, M., and Cox, J. (2016). The Perseus computational platform for comprehensive analysis of (prote)omics data. *Nat. Methods* 13, 731–740.
- Valente, E.M., Abou-Sleiman, P.M., Caputo, V., Muqit, M.M., Harvey, K., Gispert, S., Ali, Z., Del Turco, D., Bentivoglio, A.R., Healy, D.G., et al. (2004). Hereditary early-onset Parkinson's disease caused by mutations in PINK1. *Science* 304, 1158–1160.
- Wauer, T., Simicek, M., Schubert, A., and Komander, D. (2015a). Mechanism of phospho-ubiquitin-induced PARKIN activation. *Nature* 524, 370–374.
- Wauer, T., Swatek, K.N., Wagstaff, J.L., Gladkova, C., Pruneda, J.N., Michel, M.A., Gersch, M., Johnson, C.M., Freund, S.M., and Komander, D. (2015b). Ubiquitin Ser65 phosphorylation affects ubiquitin structure, chain assembly and hydrolysis. *EMBO J.* 34, 307–325.
- Wilson, M.D., Saponaro, M., Leidl, M.A., and Svejstrup, J.Q. (2012). MultiDsk: a ubiquitin-specific affinity resin. *PLoS ONE* 7, e46398.
- Yamano, K., and Youle, R.J. (2013). PINK1 is degraded through the N-end rule pathway. *Autophagy* 9, 1758–1769.
- Yamano, K., Matsuda, N., and Tanaka, K. (2016). The ubiquitin signal and autophagy: an orchestrated dance leading to mitochondrial degradation. *EMBO Rep.* 17, 300–316.
- Zhang, Y., Pak, C., Han, Y., Ahlenius, H., Zhang, Z., Chanda, S., Marro, S., Patzke, C., Acuna, C., Covy, J., et al. (2013). Rapid single-step induction of functional neurons from human pluripotent stem cells. *Neuron* 78, 785–798.
- Zhang, W., Wu, K.P., Sartori, M.A., Kamadurai, H.B., Ordureau, A., Jiang, C., Mercredi, P.Y., Murchie, R., Hu, J., Persaud, A., et al. (2016). System-Wide Modulation of HECT E3 Ligases with Selective Ubiquitin Variant Probes. *Mol. Cell* 62, 121–136.
- Zuris, J.A., Thompson, D.B., Shu, Y., Güllinger, J.P., Bessen, J.L., Hu, J.H., Maeder, M.L., Joung, J.K., Chen, Z.Y., and Liu, D.R. (2015). Cationic lipid-mediated delivery of proteins enables efficient protein-based genome editing in vitro and in vivo. *Nat. Biotechnol.* 33, 73–80.

STAR★METHODS

KEY RESOURCES TABLE

REAGENT or RESOURCE	SOURCE	IDENTIFIER
Antibodies		
Anti-MFN2	Abcam	Cat#ab124773 RRID:AB_10999860
Anti-CISD1	Proteintech	Cat#16006-1-AP; RRID:AB_2080268
Anti-PCNA	Santa-Cruz	Cat#sc-56; RRID:AB_628110
Anti-TOMM20	Santa-Cruz	Cat#sc-11415; RRID:AB_2207533
Anti-PARKIN	Santa-Cruz	Cat#sc-32282; RRID:AB_628104
Anti-PARKIN	Cell Signaling Technology	Cat#2132S RRID:AB_10693040
Anti-Ub	Dako	Cat#Z0458; RRID:AB_2315524
Anti-HA	Roche	Cat#11867423001; RRID:AB_10094468
Anti-Flag M2	Sigma-Aldrich	Cat#F1804; RRID:AB_262044
Anti-PINK1	Abgent	Cat#AM6406b; RRID:AB_2237092
Anti-pS65-Ub	Millipore	Cat#ABS1513; RRID: N/A
Anti-HSP90	Santa-Cruz	Cat#sc-69703 RRID:AB_2121191
Anti- β -Actin	Santa-Cruz	Cat#sc-69879 RRID:AB_1119529
Anti-VDAC1	Abcam	Cat#ab15895; RRID:AB_2214787
Anti-TAX1BP1	Sigma-Aldrich	Cat#HPA024432; RRID:AB_1857783
Anti-NDP52	Abcam	Cat#ab68588; RRID:AB_1640255
Anti-SQSTM1	Cell Signaling Technology	Cat#7695; RRID:AB_10949900
Anti-MAP2	Thermo Fisher Scientific	Cat#MA1-19426; RRID:AB_1076853
Anti-Rabbit IgG (H+L), HRP Conjugate	Promega	Cat# W4011; RRID:AB_430833
Anti-Mouse IgG (H+L), HRP Conjugate	Promega	Cat# W4021; RRID:AB_430834
Anti-OPTN	Sigma-Aldrich	Cat#HPA003279; RRID:AB_1079527
Monoclonal Anti-M13-horse radish peroxidase	GE Healthcare	Cat#27942101; RRID: AB_2616587
Mouse monoclonal anti-FLAG (M2)	Sigma-Aldrich	Cat#F1804; RRID: AB_262044
IRDye® 680RD Goat anti-Mouse IgG (H + L)	LI-COR Biosciences	Cat# 926-68070; RRID:AB_10956588
IRDye® 800CW Goat anti-Rabbit IgG (H + L)	LI-COR Biosciences	Cat# 926-32211; RRID:AB_62184
Bacterial and Virus Strains		
<i>Rosetta(DE3)pLysS</i> Competent Cells	Novagen	Cat#70956
Chemicals, Peptides, and Recombinant Proteins		
Custom synthetic peptides	Cell Signaling Technology	See Table S1
Oligomycin A	Sigma-Aldrich	75351

(Continued on next page)

Continued

REAGENT or RESOURCE	SOURCE	IDENTIFIER
Antimycin A	Sigma-Aldrich	A8674
CCCP	Sigma-Aldrich	C2759
Aprotinin	Roche	10981532001
Leupeptin	Roche	11017101001
AEBSF	Gold Biotechnology	A-540
TCEP	Gold Biotechnology	TCEP2
Doxycycline	Sigma-Aldrich	D9891
Puromycin	Gold Biotechnology	P-600-500
Kinetin (N6 furfuryl Adenosine 5' deoxy ribose)	Sigma-Aldrich	48130
UbV Phage Library	Zhang et al., 2016 ; Ernst et al., 2013	N/A
Halo-UBA ₄ -UBQLN1	Ordureau et al., 2014 ; This paper	N/A
Halo-UBA ₅ -DSK2	Ordureau et al., 2015 ; This paper	N/A
HaloLink Resin	Promega	G1915
Hydrogen Peroxide	Sigma-Aldrich	H1009
Formic Acid	Sigma-Aldrich	94318
DAPI	Thermo Fisher Scientific	D1306
Ubiquitin	Sigma-Aldrich	U6253
p-S65-Ubiquitin (stoichiometrically phosphorylated)	Ordureau et al., 2014	N/A
AQUApure Tetra-Ub Chains (K48-linked)	Boston Biochem (R&D systems)	UC-210B
AQUApure Phospho-Tetra-Ub Chains (K48, pS65) - (stoichiometrically phosphorylated)	Boston Biochem (R&D systems)	UC-250
AQUApure Tetra-Ub Chains (K63-linked)	Boston Biochem (R&D systems)	UC-310B
AQUApure Phospho-Tetra-Ub Chains (K63, pS65) - (stoichiometrically phosphorylated)	Boston Biochem (R&D systems)	UC-350
Critical Commercial Assays		
<i>GeneArt Precision gRNA Synthesis Kit</i>	Thermo-Fisher	A29377
Recombinant SpCas9	Zuris et al., 2015 ; This paper	N/A
Adenosine 5' triphosphate, disodium, trihydrate (ATP)	Thermo-Fisher Scientific	Cat#10326943
Brain-derived neurotrophic factor (BDNF)	Peprtech	Cat#450-02
Trysin	Promega	V511C
Lys-C	Wako Chemicals	129-02541
Guanidine HCL	Sigma-Aldrich	G3272
Rapigest SF Surfactant	Glix Laboratories	Cat#GLXC-07089
Triethyl ammonium bicarbonate (TEAB)	Sigma-Aldrich	T7408
EPPS	Sigma-Aldrich	Cat#E9502
2-Chloroacetamide	Sigma-Aldrich	C0267
PR-619	Selleck Chem	Cat#S7130
Tandem Mass Tags	Thermo Fisher Scientific	Cat#90406
Neurotrophin-3	Peprtech	Cat#450-03
Experimental Models: Cell Lines		
HeLa Flip-In T-REx (Parental line)	Brian Raught, Ontario Cancer Institute	
HeLa Flip-In T-REx PARKIN-WT	Ordureau et al., 2014 ; Ordureau et al., 2015	N/A
HeLa Flip-In T-REx PARKIN-WT; PINK1 ^{-/-}	Ordureau et al., 2014 ; Ordureau et al., 2015	N/A
HeLa Flip-In T-REx PARKIN-C341S	Ordureau et al., 2014 ; Ordureau et al., 2015	N/A
HeLa Flip-In T-REx PARKIN-S65A	Ordureau et al., 2014 ; Ordureau et al., 2015	N/A
HeLa Flip-In T-REx PARKIN-WT; mt-mKeima	Ordureau et al., 2014 ; this paper	N/A
H9 ES cells	WiCell, Madison WI	WA09
H9 ES PARKIN-S65A (homozygous)	This paper	N/A

(Continued on next page)

Continued

REAGENT or RESOURCE	SOURCE	IDENTIFIER
H9 ES PINK1 –/– (homozygous)	This paper	N/A
HUES1	Cowan et al., 2004	Harvard University Cell Repository
HUES1 PARKIN –/–	T.A., unpublished data	N/A
Oligonucleotides		
PARKIN S65A knock-in sgRNA for cutting	5'-GAACAATGCTCTGCTGATCC-3'	N/A
PINK1 deletion sgRNA_1	5'-CCGGGCGGGAGCCTCGCA-3'	N/A
PARKIN S65A knock-in replacement oligonucleotide (bases in caps indicate mutated bases)	5'-tttctggggtcgtcgcctccagttgcattca ttcttgaccttttccacggctctgcacaatg tgaacaatgGCctgctgatccaggtcacaatt ctgttgggagcaaggtaaaaaaaaaaaaaa aaaaaaaaaggaaatgcaaacatg-3'	N/A
Recombinant DNA		
pTet-O-Ngn2-puro	Addgene	52047
pET-NLS-Cas9-6xHis	Zuris et al., 2015 ; Addgene	62934
pFN18A-Halo-UBA ₄ -UBQLN1	Ordureau et al., 2014	N/A
pET-53-DEST-UbV01	This paper	N/A
pET-53-DEST-UbV02	This paper	N/A
pET-53-DEST-UbV03	This paper	N/A
pET-53-DEST-UbV04	This paper	N/A
pET-53-DEST-UbV05	This paper	N/A
pET-53-DEST-UbV06	This paper	N/A
pET-53-DEST-UbV07	This paper	N/A
pET-53-DEST-UbV08	This paper	N/A
pET-53-DEST-UbV09	This paper	N/A
pET-53-DEST-UbV10	This paper	N/A
pDONR223-UbV01	This paper	N/A
pDONR223-UbV02	This paper	N/A
pDONR223-UbV03	This paper	N/A
pDONR223-UbV04	This paper	N/A
pDONR223-UbV05	This paper	N/A
pDONR223-UbV06	This paper	N/A
pDONR223-UbV07	This paper	N/A
pDONR223-UbV08	This paper	N/A
pDONR223-UbV09	This paper	N/A
pDONR223-UbV10	This paper	N/A
pHAGE-N-term-Flag-HA-UbV01-IRES Puro	This paper	N/A
pHAGE-N-term-Flag-HA-UbV02-IRES Puro	This paper	N/A
pHAGE-N-term-Flag-HA-UbV03-IRES Puro	This paper	N/A
pHAGE-N-term-Flag-HA-UbV04-IRES Puro	This paper	N/A
pHAGE-N-term-Flag-HA-UbV05-IRES Puro	This paper	N/A
pHAGE-N-term-Flag-HA-UbV06-IRES Puro	This paper	N/A
pHAGE-N-term-Flag-HA-UbV07-IRES Puro	This paper	N/A
pHAGE-N-term-Flag-HA-UbV08-IRES Puro	This paper	N/A
pHAGE-N-term-Flag-HA-UbV09-IRES Puro	This paper	N/A
pHAGE-N-term-Flag-HA-UbV10-IRES Puro	This paper	N/A
GATWAY Destination pET-53-DEST	Millipore Sigma-Aldrich	71844
pHAGE-Mito-mKeima-IRES Puro	This paper; a gift from A. Miyawaki for the original mt-Keima construct.	

(Continued on next page)

Continued		
REAGENT or RESOURCE	SOURCE	IDENTIFIER
Software and Algorithms		
Skyline	MacLean et al., 2010	https://skyline.ms/
PyMOL	The PyMOL Molecular Graphics System, v.1.8.6.0, Schrodinger, LLC	https://pymol.org
Prism	GraphPad, v7	https://www.graphpad.com/scientific-software/prism/
Proteome Discoverer	Thermo Fisher Scientific, v2.2	https://www.thermofisher.com/order/catalog/product/OPTON-30795
In-house mass spectrometry data analysis software	Huttlin et al., 2010	N/A
SEQUEST	Eng et al., 1994	N/A
Perseus	Tyanova et al., 2016	http://www.coxdocs.org/doku.php?id=perseus:start
FlowJo	V10.4	https://www.flowjo.com
ImageQuant TL	V8.2	https://www.gelifesciences.com
Other		
Orbitrap Fusion Lumos Mass Spectrometer	ThermoFisher Scientific	Cat#IQLAAEGAAPFADBMBHQ
Easy-nLC 1200	ThermoFisher Scientific	LC140
Empore SPE Disks C18	3M - Sigma-Aldrich	66883-U
Matrigel		
Maxisorp Plates (96-well)	Sigma-Aldrich	M9410
Bio-Rad Protein Assay Dye Reagent Concentrate	Bio-Rad	#5000006
Amersham Typhoon 5 Biomolecular Imager	https://www.gelifesciences.com	# 29187191

STAR METHOD DETAILS

Cell culture, immunoblotting, and mitochondrial protein isolation

HeLa Flip-In T-REx cells (generously provided by Brian Raught, Ontario Cancer Institute) engineered to inducibly express a single copy of PARKIN^{WT}, the catalytically defective PARKIN^{C431S} mutant, or a non-phosphorylatable PARKIN^{S65A} mutant were created as described previously ([Ordureau et al., 2015](#); [Ordureau et al., 2014](#)). As we detected PARKIN, albeit in very small amounts, by immunoblotting in the parental cell line, we also employed gene-editing (see below) to remove the endogenous PARKIN gene (*PRKN*) prior to insertion of the PARKIN-expressing transgene into the Flip-In site. The indicated cells were either left untreated or depolarized with a mixture of Antimycin A (10 μ M) and Oligomycin A (5 μ M) or with the indicated amount of CCCP for the indicated time period. At the indicated times, cells were washed twice with ice cold PBS and lysed in lysis buffer (50 mM Tris/HCl pH 7.5, 1 mM EDTA, 1 mM EGTA, 50 mM NaF, 5 mM sodium pyrophosphate, 10 mM sodium 2-glycerol 1-phosphate, 1% (v/v) NP-40, 1 μ g/ml aprotinin, 1 μ g/ml leupeptin, 1 mM benzamide, 1 mM AEBSF, 10 μ M PR-619, 50 mM chloroacetamide and 1x PhosSTOP phosphatase inhibitor Cocktail (Roche)), to produce whole cell extracts.

Crude mitochondria was purified after 2 two wash in ice cold PBS by scraping cells in PBS containing 200 mM chloroacetamide (3 mL per 15 cm dish). Cells were then collected and centrifuged at 450xg for 5 minutes at 4°C. Cell pellet was resuspended in 5 mL (per 15 cm dish) mitochondrial isolation buffer (MIB) (50 mM Tris/HCl, pH 7.5, 70 mM Sucrose, 210 mM Sorbitol, 1 mM EDTA, 1 mM EGTA, 50 mM NaF, 5 mM sodium pyrophosphate, 10 mM sodium 2-glycerophosphate, 1 mM AEBSF, 10 μ M PR-619, 1 mM benzamide, 1 μ g/ml leupeptin and aprotinin) plus 100 mM chloroacetamide and centrifuged at 1400xg for 5 minutes at 4°C. The cell pellet was re-suspended in 5 mL MIB buffer plus 100 mM chloroacetamide and sonicated twice for 10 s at lowest settings. Sample were spun 10 min at 1400xg to remove unbroken cells/debris and supernatant was collected, this correspond to the “total protein” fraction, and transferred into round-bottom tube prior to centrifugation for 10 min at 10000xg at 4°C. Supernatant which correspond to cytosolic fraction and crude ER fraction was removed and the pellet corresponding to the crude mitochondria fraction was resuspended in 10 mL of MIB buffer plus 50 mM chloroacetamide, prior to centrifugation for 10 min at 10000xg. The mitochondrial pellet was wash two more time and pellet was then lysed in lysis buffer.

Whole cell extracts or mitochondrial extracts were sonicated and clarified by centrifugation (16000xg for 10 min at 4°C) followed by filtration through a 0.45 μ M filter and protein concentrations determined by the Bradford assay. Cell extracts (25 μ g or 50 μ g for p-S65-Ub immunoblotting) or mitochondrial extracts were separated by SDS/PAGE, transferred to PVDF membranes, and proteins detected by immunoblotting.

Mitochondrial poly-ubiquitin capture and proteomics

Mitochondrially-derived ubiquitylated proteins were purified from the indicated HeLa cells or hESC-derived neurons using Halo-4xUBA^{UBQLN1} and Halo-5xUBA^{DSK2} resin (referred to as immobilized UBA resin in the main text), produced as previously described (Ordureau et al., 2015; Ordureau et al., 2014). Briefly, whole cell extracts (using 0.5 mg unless indicated otherwise) or mitochondrial extracts (using 0.25 mg unless indicated otherwise) were lysed in lysis buffer containing 50 μ M chloroacetamide prior to incubation at 4°C for 16 h with 30–50 μ L of Halo-4xUBA^{UBQLN1} beads (pack volume). Subsequently, the supernatant was incubated with 15 μ L of Halo-5xUBA^{DSK2} for 2 hours to capture any possible residual mono-ubiquitylated proteins (Ordureau et al., 2015; Wilson et al., 2012). Halo beads were combined and following 4 washes with lysis buffer containing 0.5 M NaCl and one final wash in 10 mM Tris pH 8.0, proteins were released from the Halo-UBA resin using sample buffer prior to analysis by SDS-PAGE and immunoblotting or by 6M Guanidine HCL when analyzed by mass spectrometry. For immunoblotting, samples were separated on 4%–12% Bis-Tris gradient gels. For mass spectrometry, samples were subjected to reduction (5 mM tris (2-carboxyethyl)phosphine (TCEP) for 10 min at room temperature) and alkylation (25 mM chloroacetamide for 20 min at room temperature) followed by Trichloroacetic Acid (TCA) precipitation and 3 washes with ice cold acetone. Samples were dried and resuspended in 30 μ L digestion buffer (100 mM triethyl ammonium bicarbonate pH 8.5, 0.1% RapiGest, 10% ACN) and digested for 2 h at 37°C with Lys-C and then a further 6–8 h with trypsin at 37°C. Digests were acidified with equal volume of 1% formic acid (FA) to a pH \sim 2, incubated for 15 min, dried down, resuspended in 50 μ L 1% FA, and subjected to C18 StageTip desalting. Samples were analyzed by LC-MS/MS or used for AQUA/PRM as described below.

Heavy reference peptides and characterization

Heavy reference peptides (Table S1) for parallel reaction monitoring containing a single ¹³C/¹⁵N-labeled amino acid were synthesized, purified by reversed-phase chromatography and quantified by amino acid analysis by Cell Signaling Technologies. Heavy reference peptides from working stocks (in 5% FA / 5%ACN) were diluted into the digested sample (in 1% FA) to be analyzed to an optimal final concentration predetermined for individual peptides. LC retention times, precursor ion to be targeted, isolation window, AGC target, fill time were determined for each peptide (Table S1). A mixture of all Kgg peptides was used to determine the best ACN gradient to minimize peptide overlap during elution in a 90-min gradient. Samples and heavy reference peptides were oxidized with 0.1% hydrogen peroxide for 30 min, subjected to C18 StageTip desalting and hydrogen peroxide removal, and resuspended in 5% FA. Mass spectrometry was performed in triplicate, unless indicated otherwise, and analyzed sequentially by LC-MS on a Orbitrap Fusion Lumos instrument coupled to an Easy-nLC 1200 (Thermo Fisher Scientific) ultra-high-pressure liquid chromatography (UHPLC) pump. Peptides were separated on a 100 μ m inner diameter microcapillary column packed in house with \sim 35 cm of Accucore150 resin (2.6 μ m, 150 Å, ThermoFisher Scientific, San Jose, CA). The column was equilibrated with buffer A (3% ACN + 0.125% FA). Peptides were loaded onto the column at 100% buffer A. Separation and elution from the column was achieved using a 90-min 3%–28% gradient of buffer B (100% ACN + 0.125% FA) at \sim 500 nL/min. The total LC-method with loading, separation, and column equilibration was 110 min. The scan sequence began with FTMS¹ spectra (resolution of 120,000; mass range 300–1000 m/z; automatic gain control (AGC) target 1×10^6 , max injection time of 100 ms). The second scan sequence consisted of a targeted-MS² (tMS²) method where MS² precursors of interested as defined in the “Mass List Table” (Table S1) were isolated using the quadrupole and analyzed in the Orbitrap (FTMS²) with an isolation window, resolution, AGC target and a max injection time defined in the “Mass List Table” (Table S1). MS² precursors were fragmented by HCD at a normalized collision energy (NCE) of 32%. For measurement of the protein amount in mitochondrial extracts, unmodified peptides corresponding to the various proteins of interest were analyzed with the multiplexing (MSX) option set to the equal fill time mode (MSX = 2; AGC 1×10^5 (total); injection time of 108 ms total) Instrument methods with detailed parameters for the two Pt-PRM iterations can be found in Data S1 (mito prep) and Data S2 (Halo-UBA enriched mitochondria). LC-MS data analysis was performed using Skyline software (MacLean et al., 2010) with manual validation of precursors and fragments. The results exported to Excel and GraphPad Prism for further analysis and plotting (Table S1).

Proteomics – Label-free Analysis

Label-free analysis was performed in triplicate (duplicate for DA neurons) and analyzed sequentially by LC/MS². All spectra were acquired on an Orbitrap Fusion or Lumos mass spectrometer (Thermo Fisher Scientific) coupled to an Easy-nLC 1200 (Thermo Fisher Scientific) ultra-high-pressure liquid chromatography (UHPLC) pump. Peptides were separated on a 100 μ m inner diameter microcapillary column packed in house with \sim 35 cm of Accucore150 resin (2.6 μ m, 150 Å, ThermoFisher Scientific, San Jose, CA) with a gradient consisting of 5%–28% (ACN, 0.1% FA) over 150 min at \sim 500 nL/min. The scan sequence began with FTMS¹ spectra (resolution of 120,000; mass range 400–1400 m/z; automatic gain control (AGC) target 1×10^6 , max injection time of 100 ms). The most intense MS¹ ions were selected for MS² analysis, using TopSpeed method with total cycle time of 3 s. Precursors were filtered according to charge state ≥ 2 and ≤ 6 . Monoisotopic peak assignment was used, and previously interrogated precursors were excluded using a dynamic window (120 s \pm 7 ppm). Minimum intensity to trigger an MS² scan was 2×10^4 . MS² precursors were isolated using the quadrupole (1.2 Th window) and analyzed in the Orbitrap (FTMS²) at 15,000 resolution, with an AGC target of 5×10^4 and a max injection time of 118 ms. Precursors were fragmented by HCD at a normalized collision energy (NCE) of 32%. Mass spectra were processed using Protein Discoverer version 2.2 (Thermo Fisher Scientific) using the Minora algorithm (set to default parameters). The identification of proteins was performed using the SEQUEST-HT engine against the UniProt Human Reference Proteome (2017) using the following parameters: a tolerance level of 20 ppm for MS¹ and 0.03 Da for MS² and false discovery rate of the

Percolator decoy database search was set to 1%. Trypsin was used as the digestion enzyme, three missed cleavages were allowed, and the minimal peptide length was set to 6 amino acids. The carbamidomethylation of cysteine was set as a fixed modification, and the oxidation of methionine was allowed as a variable modification. Proteins with less than two unique peptides were filtered out and only unique peptides were used for quantification (precursor abundance based on area). Protein with more than 20% CV across replicates were discarded. Label-free abundance calculated were normalized across samples to total peptide amount of mitochondrial protein (MitoCarta 2.0). The following database containing mitochondrial protein were used: MitoCarta 2.0 (Calvo et al., 2016), Integrated Mitochondrial Protein Index (IMPI Q3 2017 – using only validate proteins (1128) - <http://www.mrc-mbu.cam.ac.uk/impi>) and the Mitochondrial Outer Membrane (MOM) dataset from (Hung et al., 2017). Proteins not present in any of the 3 databases (non-mitochondrial proteins) were filtered out.

Proteomics – TMT Quantification

Mitochondrial protein extracts were subjected to disulfide bond reduction with 5 mM TCEP (room temperature, 10 min) and alkylation with 25 mM chloroacetamide (room temperature, 20 min). TCA precipitation was performed prior to protease digestion. Samples were resuspended in 100 mM EPPS, pH 8.5 and digested at 37°C for 4h with LysC protease at a 200:1 protein-to-protease ratio. Trypsin was then added at a 100:1 protein-to-protease ratio and the reaction was incubated for 6 h at 37°C. Tandem mass tag labeling was performed as follow, in brief, ~5 µg of digested peptides, resuspended in 50 µL of 0.1 M EPPS (pH 8.5) from each sample were labeled with TMT reagent. A total of 2 µL of the 20 ng/µL stock of TMT reagent was added to the peptides along with 12.5 µL of acetonitrile to achieve a final acetonitrile concentration of approximately 20% (v/v). Following incubation at room temperature for 1 h, the reaction was quenched with hydroxylamine to a final concentration of 0.5% (v/v) for 15 min. The TMT-labeled samples were pooled together at a 1:1 ratio. The sample was vacuum centrifuged to near dryness, fractionated according to manufacturer's instructions using High pH reversed-phase peptide fractionation kit (Thermo Fisher Scientific) and subjected to C18 solid-phase extraction (SPE) (Sep-Pak, Waters).

Mass spectrometry data were collected using an Orbitrap Fusion Lumos mass spectrometer (Thermo Fisher Scientific, San Jose, CA) coupled to a Proxeon EASY-nLC1200 liquid chromatography (LC) pump (Thermo Fisher Scientific). Peptides were separated on a 100 µm inner diameter microcapillary column packed in house with ~35 cm of Accucore150 resin (2.6 µm, 150 Å, ThermoFisher Scientific, San Jose, CA) with a gradient consisting of 5%–23% (ACN, 0.1% FA) over 150 min at ~500 nL/min. For analysis, we loaded ~2 µg of each fraction onto the column. Each analysis used the Multi-Notch MS³-based TMT method (McAlister et al., 2014), to reduce ion interference compared to MS² quantification. The scan sequence began with an MS¹ spectrum (Orbitrap analysis; resolution 120,000 at 200 Th; mass range 400–1350 m/z; automatic gain control (AGC) target 1×10^6 ; maximum injection time 100 ms). Precursors for MS² analysis were selected using a Top10 method. MS² analysis consisted of collision-induced dissociation (quadrupole ion trap analysis; Turbo scan rate; AGC 2.5×10^4 ; normalized collision energy (NCE) 35; maximum injection time 150 ms). Monoisotopic peak assignment was used and previously interrogated precursors were excluded using a dynamic window (120 s ± 5 ppm). Following acquisition of each MS² spectrum, a synchronous-precursor-selection (SPS) MS³ scan was collected on the top 10 most intense ions in the MS² spectrum (McAlister et al., 2014). MS³ precursors were fragmented by high energy collision-induced dissociation (HCD) and analyzed using the Orbitrap (NCE 65; AGC 1.5×10^5 ; maximum injection time 150 ms, resolution was 50,000 at 200 Th).

Mass spectra were processed using a Proteome Discoverer 2.2 (Thermo Fisher Scientific). The identification of proteins was performed using the SEQUEST-HT engine against the UniProt Human Reference Proteome (2017) using the following parameters: a tolerance level of 15 ppm for MS¹ and 0.7 Da for MS² and false discovery rate of the Percolator decoy database search was set to 1%. Trypsin was used as the digestion enzyme, three missed cleavages were allowed, and the minimal peptide length was set to 6 amino acids. TMT tags on lysine residues and peptide N termini (+229.163 Da) and carbamidomethylation of cysteine residues (+57.021 Da) were set as static modifications, while oxidation of methionine residues (+15.995 Da) and Phosphorylation of serine (+79.966 Da) was set as a variable modification. Scoring and localization of phosphorylation site was done using the ptmRS node (default settings). For TMT-based reporter ion quantitation, we extracted (integration tolerance of 0.003 Da) the summed signal-to-noise ratio for each TMT channel and found the closest matching centroid to the expected mass of the TMT reporter ion. For protein-level comparisons, PSMs were identified, quantified, and collapsed to a 1% peptide false discovery rate (FDR) and then collapsed further to a final protein-level FDR of 1%. Moreover, protein assembly was guided by principles of parsimony to produce the smallest set of proteins necessary to account for all observed peptides. Proteins were quantified by summing reporter ion counts across all matching PSMs for unique peptides only. PSMs with poor quality, MS³ spectra with more than eight TMT reporter ion channels missing, MS³ spectra with TMT reporter summed signal-to-noise ratio that were less than 100, isolation specificity ≤ 0.7 , or had no MS³ spectra were excluded from quantification (McAlister et al., 2012). Protein quantification values were exported for further analysis in Microsoft Excel and GraphPad Prism for plotting. Each reporter ion channel was summed across all quantified proteins and normalized assuming equal protein loading of all 10 samples.

Comparison of pS65-Ub and Ub chain linkages in crude versus sucrose density gradient purified mitochondria

Using crude and sucrose density gradient purified mitochondria from HeLa Flip-In T-REx-PARKIN^{WT} cells (16 h DOX treatment to induce PARKIN) with and without AO (1h) purified as described (Ordureau et al., 2014), we determined that 15.95 and 17.78% of Ub chains were phosphorylated on S65 in crude and sucrose gradient purified mitochondria after depolarization, in range with

what was previously reported (Ordureau et al., 2015; Ordureau et al., 2014). Moreover, the chain linkage types and fold-change upon depolarization were similar, as seen previously (Ordureau et al., 2015; Ordureau et al., 2014). We also subjected crude and sucrose density gradient purified mitochondria to immunoblotting (ran on 4%–20% Bis-Tris SDS-PAGE gels with MES buffer to retain monomeric Ub and transferred to 0.2 μ m PVDF membrane) with α -Ub and α -pS65-Ub antibodies. Approximately 10%–15% of the Ub signal, the majority of which migrated as a high molecular weight smear, migrated at the position of free monomeric Ub in both the crude and sucrose gradient purified mitochondria, but this free Ub was not detected in the phosphorylated form by immunoblotting, suggesting that the vast majority of the pS65-Ub signal was in the form of conjugates. This suggests that the fraction of pS65-Ub in Ub chains on mitochondria calculated from either crude or sucrose gradient purified may be under-estimated by ~10%–15%.

Gene-Editing and differentiation

Human ES cells (H9, WiCell Institute) were cultured in E8 medium (Chen et al., 2011) on Matrigel-coated tissue culture plates with daily medium change. Cells were passaged every 4–5 days with 0.5 mM EDTA in 1 \times DPBS (Thermo Fisher Scientific). The SpCas9 expression plasmid pET-NLS-Cas9-6xHis (Addgene plasmid # 62934) was transformed into *Rosetta(DE3)pLysS* Competent Cells (Novagen). SpCas9 protein was purified as described elsewhere (Zuris et al., 2015). The sgRNAs were generated using *GeneArt Precision gRNA Synthesis Kit* (Thermo Fisher Scientific) according to the manufacturer's instruction and purified using RNeasy Mini Kit (QIAGEN). The sgRNA target sequences were: PARKIN S65A, GAACAATGCTCTGCTGATCC; PINK1^{-/-}, CCGGGCGCGGAGC CTCGCA and GCTAGGGCTGGGCCTCATCG.

To generate PINK1^{-/-} cells, 0.6 μ g sgRNA was incubated with 3 μ g SpCas9 protein for 10 minutes at room temperature and electroporated into 2 \times 10⁵ H9 cells using Neon transfection system (Thermo Fisher Scientific). To create H9 cells harboring a homozygous S65A mutation in PARKIN, a ssDNA oligo (tttctggggtcgtcgctccagttgcattcatttctgaccttttctccacggtcctcgcacaatgtgaacaatgGCctgct gatccaggtcacaattctgtttgggagcaaggtaaaaaaaaaaaaaaaaaaggaaatgtcaaacatg) was electroporated into H9 cells along with the Cas9/sgRNA complex. Mutants were identified by Illumina MiSeq and further confirmed by Sanger sequencing for PARKIN^{S65A} or by western blot for PINK1^{-/-} mutants. PARKIN^{-/-} ES cells (H9 or HUES1, (Cowan et al., 2004) were created in exon 3 using sgRNA GGCGACGACCCCAGAAACG or a combination of GGAGCCCCAGAGCTTGACTC and GGTCAGAAATGAATGCAAC, respectively. Out of frame deletions were verified by DNA sequencing with Illumina MiSeq and by immunoblotting. The PARKIN locus in HeLa Flip-In T-REX cells was deleted using CRISPR/Cas9 with the guide sequence GTGTCAGAATCGACCTCCAC, which cuts in exon 2 (near F13 in PARKIN's UBL) and the absence of expression confirmed by immunoblotting.

For human ES cell conversion to iNeurons, cells were transduced with lentiviruses generated using pTet-O-Ngn2-puro (Addgene plasmid # 52047) and FUDeltaGW-rTA (Addgene plasmid #19780) at MOI 5, respectively, and induced as described (Zhang et al., 2013) with modification. Briefly, lentivirus-transduced human ES cells were expanded and plated at 2–2.5 \times 10⁴/cm² on Matrigel-coated tissue plates in DMEM/F12 supplemented with 1 \times N2, 1 \times NEAA (Thermo Fisher Scientific), human BDNF (10 ng/ml, PeproTech), human NT-3 (10 ng/ml, PeproTech), mouse laminin (0.2 μ g/ml, Cultrex), Y-27632 (10 μ M, PeproTech) and Doxycycline (2 μ g/ml, Alfa Aesar) on Day 0. On Day 1, Y-27632 was withdrawn and puromycin (1 μ g/ml, Thermo Fisher Scientific) was added. On Day 2, medium was replaced with Neurobasal medium supplemented with 1 \times B27 and 1 \times Glutamax (Thermo Fisher Scientific) containing Brain-derived neurotrophic factor (BDNF), Neurotrophin-3 (NT-3), puromycin and Doxycycline. Puromycin was withdrawn on Day 4 and half of the medium was replaced every other day thereafter. Dopaminergic neurospheres were produced as described (Rigamonti et al., 2016).

Mitophagy assays

Cell lines of interest were infected with lentivirus encoding for mitochondrial matrix targeted mKeima (mito-mKeima) and selected with puromycin. After several passages, cells were FACS sorted into a uniform population (intensity) for the mito-mKeima. The indicated cell line grown in 12-well plates were treated with doxycycline (0.1 μ M) for 16 h to induce PARKIN and then treated with CCCP (10 μ M or 1 μ M) for the indicated time and collected after trypsin treatment. After re-suspending the cells in a FACS buffer (1 \times DPBS, 1 mM EDTA, 1% FBS, 25 mM HEPES, 1 μ g/ml DAPI, final pH 7.3–7.5), the reconstituted cells were filtered through the cell strainer into the 5ml test tube (Corning, 352235). The cells were analyzed by flow-cytometry (MoFlo Astrios EQ, Beckman Coulter). The data was processed by FlowJo software, with the following gating strategies: 1. Single cells were gated by SSC1 height/FSC1 height followed by SSC1 height/SSC1-width. 2. Live cells were sorted by 405–448 (DAPI positive)/SSC1 height. 3. mKeima positive cells were gated by 488ex/620em and 561ex/614em. The mean 561 ex/614em and 488ex/620em values of 10,000 cells were obtained in FlowJo Table Editor, and the 561/488 ratio was calculated and exported into Prism software for plotting.

Selection of UbVs for PARKIN

The phage-displayed Ub variant (UbV) library used for selection was re-amplified from Library 2 as previously described (Ernst et al., 2013). Protein immobilization and the following phage selections were done according to standard protocols (Tonikian et al., 2007). Briefly, purified PARKIN^{295–465} were coated on 96-well MaxiSorp plates by adding 100 μ L of 1 μ M proteins and incubating overnight at 4°C. In the following days, five rounds of phage display selections were performed as follows: a) Preparation of the phage library pool, within which each phage particle displays a unique UbV and encapsulates the encoding DNA; b) The pool of phage displayed UbV library are applied to immobilized PARKIN; c) PARKIN-binding phage are captured and non-binding phage are washed away; d) Bound phage are amplified by infection of bacterial host *Escherichia coli*; e) Individual phage with improved binding properties

obtained from round 4 and round 5 are identified by phage ELISA (see below) and subjected to DNA sequencing of the phagemids to obtain UbV sequences (Zhang et al., 2016).

ELISA to evaluate UbV binding and specificity

Phage and protein ELISA against immobilized proteins was performed as previously described (Zhang et al., 2016). Briefly, PARKIN proteins and other controls as indicated (1 μ M) were individually immobilized in microtiter plates (30 μ l). Binding of phage was detected using anti-M13-HRP antibody and colorimetric development of TMB peroxidase substrate. Purified PARKIN UbVs were added in the concentration of 10 μ M for competitive ELISA to test for potential displacement of UbV phage binding. For protein ELISA to measure the half maximal binding concentration (EC_{50}) of UbVs binding to proteins under study, two-fold serial dilutions of FLAG-tagged UbV or Ub (starting at 4 μ M, 24 points, 30 μ l) were added and incubated for 20 min at room temperature. Wells were washed and bound UbV was detected by anti-FLAG-HRP conjugate antibody and colorimetric development of TMB peroxidase substrate.

Analysis of UbV activity *in vitro* and *in vivo*

To examine the effect of PARKIN-binding UbVs on Ub ligase activity, PARKIN (1 μ M) was phosphorylated with TcPINK1 as described (Ordureau et al., 2014) and reactions mixtures supplemented with the indicated FLAG-UbV (5 μ M), Ub (7.5 μ M), E1 (100 nM), UBCH7 (500 nM), and ATP (1 mM). After 1 h, reaction mixtures were separated by SDS-PAGE and immunoblotted with either α -Ub or α -FLAG. To examine UbV activity in cells, the indicated UbVs in pDONR223 (Rual et al., 2004) were transferred to pHAGE-N-term-Flag-HA-IRES-Puro vectors and were stably expressed in HeLa-Flip-In T-REx PARKIN cells expressing the indicated WT or mutant PARKIN and in some cases gene edited to delete PINK1 (Ordureau et al., 2015; Ordureau et al., 2014). PARKIN proteins were induced with Dox (1 μ M, 16h), cells depolarized for 1 or 4h, and cells harvested for either immunoblotting of purified mitochondria or PRM analysis for primary substrates and pS65-Ub. Expression of FLAG-UbVs was verified by immunoblotting of cell extracts. To examine inhibition of PARKIN recruitment to mitochondria, we expressed GFP-PARKIN stably in HeLa Flip-In T-REx cells expressing individual FLAG-UbVs (puromycin selection) and 1 h after depolarization, we performed immunofluorescence using a-TOMM20 antibodies and imaging as previously described (Ordureau et al., 2015; Ordureau et al., 2014).

Analysis of Kinetin activity *in vivo*

To examine the effect of Kinetin (Hertz et al., 2013) on PINK1 downstream signaling HeLa-Flip-In T-REx cells expressing the indicated WT or mutant PARKIN and in some cases gene edited to delete PINK1 (Ordureau et al., 2015; Ordureau et al., 2014) were used. Kinetin was dissolved prior to usage in DMSO at 50 mM and sonicated for 5 min in water bath at 37°C. To examine Kinetin activity in cells, cells were pre-treated for 4-6 days with at a final concentration of 50 μ M Kinetin and media was renewed with Kinetin every 48 hr. PARKIN proteins were induced with Dox (0.5 μ M, 16h), cells depolarized for the indicated time with the indicated amount of CCCP and harvested for either immunoblotting of purified mitochondria or PRM analysis for pS65-Ub and VDACS Kgg.

Structural modeling

MOM protein structures were from previously reported crystal structure where available: CISD1 (3EW0), VDAC1 (2JK4), HK1 (4F9O), RHOT1 (5KSZ). Models for other proteins were generated in SWISS-MODEL (<https://swissmodel.expasy.org/interactive>) using the following templates: CISD2 (CISD1, 3EW0); VDAC2 (*D.r.* VDAC1, 4BUM); VDAC3 (*D.r.* VDAC1, 4BUM); FKBP8 (FKBP38, 5MGX); MFN1 (mini-MFN, 5GNU); MFN2 (mini-MFN, 5GNU); TOMM70 (*S.c.* Tom70, 2GW1); MUL1 RING domain (MDM2 RING domain, 5MNJ); RHOT2 (RHOT1, 5KSZ). Structures were rendered in Pymol (<https://pymol.org>).

QUANTIFICATION AND STATISTICAL ANALYSIS

Unless stated otherwise all quantitative experiments were performed in triplicate and average with standard error of the mean (SEM) reported.

CONTACT FOR REAGENT AND RESOURCE SHARING

Further information and requests for resources and reagents should be directed to and will be fulfilled by the Lead Contact, J. Wade Harper (wade_harper@hms.harvard.edu).